The Journal of Physiology

Role of capillary pericytes in the integration of spontaneous Ca^{2+} transients in the suburothelial microvasculature *in situ* of the mouse bladder

Hikaru Hashitani, Retsu Mitsui, Kyoko Miwa-Nishimura and Michelle Lam

Department of Cell Physiology, Graduate School of Medical Sciences, Nagoya City University, Nagoya, Japan

Edited by: Laura Bennet and Kim Dora

Key points

- In the bladder suburothelial microvasculature, pericytes in different microvascular segments develop spontaneous Ca^{2+} transients with or without associated constrictions.
- Spontaneous Ca^{2+} transients in pericytes of all microvascular segments primarily rely on the cycles of Ca^{2+} uptake and release by the sarco- and endoplasmic reticulum.
- The synchrony of spontaneous Ca^{2+} transients in capillary pericytes exclusively relies on the spread of depolarizations resulting from the opening of Ca^{2+}-activated chloride channels (CaCCs) via gap junctions.
- CaCC-dependent depolarizations further activate L-type voltage-dependent Ca^{2+} channels as required for the synchrony of Ca^{2+} transients in pericytes of pre-capillary arterioles, post-capillary venules and venules.
- Capillary pericytes may drive spontaneous Ca^{2+} transients in pericytes within the suburothelial microvascular network by sending CaCC-dependent depolarizations via gap junctions.

Abstract Mural cells in the microvasculature of visceral organs develop spontaneous Ca^{2+} transients. However, the mechanisms underlying the integration of these Ca^{2+} transients within a microvascular unit remain to be clarified. In the present study, the origin of spontaneous Ca^{2+} transients and their propagation in the bladder suburothelial microvasculature were explored. Cal-520 fluorescence Ca^{2+} imaging and immunohistochemistry were carried out on mural cells using mice expressing red fluorescent protein (DsRed) under control of the NG2 promotor. NG2(+) pericytes in both pre-capillary arterioles (PCAs) and capillaries developed synchronous spontaneous Ca^{2+} transients. By contrast, although NG2-DsRed also labelled arteriolar smooth muscle cells, these cells remained quiescent. Both NG2(+) pericytes in post-capillary

Hikaru Hashitani has been a Professor of Cell Physiology at Nagoya City University Graduate School of Medical Sciences since 2010. He received his medical degree from Kyushu University in 1991 and completed his PhD at Nagoya City University in 1997. He undertook postdoctoral research at Melbourne University from 1997 to 1999 and at University of Oxford from 2000 to 2002. His primary research focus is the cellular mechanisms underlying the initiation and the propagation of spontaneous electrical and calcium signalling in smooth muscle, particularly of the urinary tract. More recently, his research interest has extended to the roles of pericytes in generating spontaneous activity in the microvasculature.

DOI: 10.1113/JP275845

venules (PCVs) and NG2(–) venular pericytes exhibited propagated Ca^{2+} transients. L-type voltage-dependent Ca^{2+} channel (LVDCC) blockade with nifedipine prevented Ca^{2+} transients or disrupted their synchrony in PCA, PCV and venular pericytes without dis-synchronizing Ca^{2+} transients in capillary pericytes. Blockade of gap junctions with carbenoxolone or Ca^{2+}-activated chloride channels (CaCCs) with 4,4′-diisothiocyanato-2,2′-stilbenedisulphonic acid disodium salt prevented Ca^{2+} transients in PCA and venular pericytes and disrupted the synchrony of Ca^{2+} transients in capillary and PCV pericytes. Spontaneous Ca^{2+} transients in pericytes of all microvascular segments were abolished or suppressed by cyclopiazonic acid, caffeine or tetracaine. The synchrony of Ca^{2+} transients in capillary pericytes arising from spontaneous Ca^{2+} release from the sarco- and endoplasmic reticulum appears to rely exclusively on CaCC activation, whereas subsequent LVDCC activation is required for the synchrony of Ca^{2+} transients in pericytes of other microvascular segments. Capillary pericytes may drive spontaneous activity in the suburothelial microvascular unit to facilitate capillary perfusion.

(Resubmitted 22 March 2018; accepted after revision 21 May 2018; first published online 26 May 2018)
Corresponding author H. Hashitani: Department of Cell Physiology, Nagoya City University Graduate School of Medical Sciences, Nagoya 467-8601, Japan. Email: hasitani@med.nagoya-cu.ac.jp

Introduction

The microvasculature, consisting of arterioles, capillaries and venules, functions as an integrated unit to maintain microcirculation. The microcirculation serves to regulate blood flow and tissue perfusion, thereby ensuring the delivery of oxygen and nutrients to meet the tissue demands, as well as the removal of tissue metabolites. Traditionally, arterioles are considered to play a predominant role in controlling the vascular resistance and hence the distribution and rate of blood flow into individual organs or tissues, whereas substance exchange between the blood flow and tissues primarily occurs across the wall of capillaries. Because capillary filtration and reabsorption is a function of hydrostatic pressure that is determined by the gradient of arteriolar and venular pressures, changes in the contractile properties of arterioles and venules are a determinant of capillary exchange. Capillary perfusion in different regions in individual tissues is regulated precisely to meet the energetic demands of neighbouring metabolically active cells; thus, there is considerable heterogeneity of capillary perfusions even within the same tissues (Ellis *et al.* 1994; Villringer *et al.* 1994). There is growing evidence indicating that capillaries play a more active role in regulating regional blood flow than previously assumed.

Arterioles or venules are surrounded by contractile smooth muscle cells (SMCs), whereas capillaries and pre- and post-capillary microvessels are covered by morphologically distinct pericytes. Capillary pericytes are often non-contractile and do not express α-smooth muscle actin (α-SMA) (Borysova *et al.* 2013; Burdyga & Borysova, 2014; Hill *et al.* 2015). Nevertheless, capillary pericytes in several vascular beds of the CNS play an active role in regulating capillary diameter and blood flow (Peppiatt *et al.* 2006; Femández-Klett *et al.* 2010; Hall *et al.* 2014). In addition, the dilatory signals generated in capillary pericytes appear to spread to upstream arterioles to facilitate capillary perfusion (Ishizaki *et al.* 2009; Hall *et al.* 2014). Indeed, electrical signals evoked in capillary pericytes in the retina are effectively transmitted not only to pericytes within the capillary network, but also to arterioles via gap junctions (Kawamura *et al.* 2003; Zhang *et al.* 2011). Thus, capillary pericytes may well sense neighbouring neuronal activity or metabolic conditions to generate hyperpolarizations that are transmitted to arterioles to inhibit L-type voltage-dependent Ca^{2+} channels resulting in active hyperaemia (Ishizaki *et al.* 2009; Hall *et al.* 2014; Mishra *et al.* 2016).

Besides the neuronal or metabolic regulations of microvascular contractility, a number of microblood vessels, particularly arterioles, in different microvascular beds develop spontaneous phasic constrictions, namely spontaneous vasomotion (Aalkjær & Nilsen, 2005). Vasomotion is considered to play a critical role in regulating microcirculation and thus facilitate capillary-tissue exchange (Sakurai & Terui, 2006). In several visceral organs that undergo considerable wall distention upon filling, such as the urinary bladder (Hashitani *et al.* 2011; Hashitani *et al.* 2012; Shimizu *et al.* 2014), stomach (Mitsui & Hashitani, 2015, 2016) and colon (Mitsui *et al.* 2013), pericytes or SMCs in venules display spontaneous Ca^{2+} transients and associated constrictions that may facilitate venular drainage (Dongaonkar *et al.* 2012), whereas the arterioles remain quiescent. However, arterioles in the stomach or rectum are spontaneously active and may be driven by capillary pericytes (Hashitani *et al.*, 2015; Mitsui & Hashitani, 2017). Thus, despite the fact that the microvascular network appears to function as an integrated unit as a result of electrical coupling between mural cells in different segments (Borysova *et al.* 2013), the spread of spontaneous activity within the

microvasculature may vary in a vascular bed-dependent manner. Of particular interest is whether capillary pericytes drive the spontaneous activity in other microvascular segments, and how the capillary-derived signals may spread to the arterioles or venules differently.

To understand the role of capillary pericytes in driving the spread of spontaneous activity within the microvascular unit, spontaneous Ca^{2+} signals of mural cells were visualized in different segments of the suburothelial microvasculature of mice expressing red fluorescent protein (DsRed) under control of the proteoglycan NG2 promoter (Zhu *et al.* 2008). Spontaneous Ca^{2+} transients were generated in NG2(+) pericytes of pre-capillary arterioles (PCA) and capillaries that expressed NG2-DsRed florescence, weakly NG2(+) pericytes in post-capillary venules (PCV), and NG2 negative [NG2(–)] venular pericytes. We investigated the mechanisms underlying the synchrony of spontaneous Ca^{2+} transients amongst mural cells in the same segments or their spread to adjacent segments, focusing particularly on the role of voltage-dependent Ca^{2+} channel (VDCCs), Ca^{2+}-activated chloride channels (CaCCs) and gap junctions. Microvascular contractility, expression of (α-SMA) and sympathetic innervation were also compared amongst differences microvascular segments.

Methods

Ethical approval

All experiments were approved by The Experimental Animal Committee of the Nagoya City University Graduate School of Medical Sciences (Approval no: H25M-36) prior to commencement. The experiments were carried out in accordance with the Care and Use of Animals in the Field of Physiological Sciences set out by the Physiological Society of Japan (2015) and conform with the principles and regulations described in Grundy (2015).

Animals

NG2 DsRed mice expressing a red fluorescent protein variant (DsRed.T1) under the control of the neural/glial antigen-2 expression (NG2) chondroitin sulphate proteoglycan 4 (Cspg4) promoter (Zhu *et al.* 2008) were purchased from Jackson Labs (Bar Harbor, ME, USA) [stock Tg(Cspg4-DsRed.T1)1Akik/J] and maintained hemizygous. C57BL/6J mice, aged 7–12 weeks, were purchased from Japan SLC, Inc. (Hamamatsu, Japan). Mice were housed under a 12:12 h light/dark cycle at 23 ± 1°C with free access to food and water.

Tissue preparation

Mice of both sexes, aged 7–12 weeks, were anaesthetized by exposition to vapours of isoflurane and then exsanguinated by decapitation. The bladder was removed and pinned out in a dissecting dish with the mucosal side uppermost. The mucosal layer was dissected away from the detrusor smooth muscle layer, and then the urothelial layer was carefully removed using ophthalmology scissors leaving the suburothelial layer containing the microvasculature (i.e. lamina propria).

For immunohistochemistry, the bladder was excised from NG2 DsRed mice or their non-carrier sibling, cut open and immediately immersed in PBS at 4°C.

Intracellular calcium imaging

For intracellular calcium imaging, NG2 DsRed mice were used to identify vascular mural cells in the different microvasculature segments. The lamina propria preparations, ~5 mm square, were prepared, pinned out on a Sylgard plate (silicone elastomer; Dow Corning Corporation, Midland, MI, USA) at the bottom of the recording chamber (volume, ~1 mL), superfused with warmed physiological salt solution (36°C) (PSS) at a constant flow rate (2 mL min^{-1}) and equilibrated for 60 min.

To visualize Ca^{2+} transients in the microvasculature, preparations were incubated in low Ca^{2+} PSS ($[Ca^{2+}]_o = 0.1$ mM) containing 1 μM Cal-520 AM (AAT Bioquest Inc., Sunnyvale, CA, USA) and cremophor EL (0.01%; Sigma, St Louis, MO, USA) for 10–15 min at 35°C and then for 10 min at room temperature.

Following incubation, the recording chamber was mounted on the stage of an upright epifluorescence microscope (BX51WI; Olympus, Tokyo, Japan) equipped with a back-thinned electron multiplying CCD camera (C9100-13; Hamamatsu Photonics, Hamamatsu, Japan). Preparations were superfused with dye-free PSS containing 2.5 mM Ca^{2+}, viewed with a water immersion objective (UMPlanFL 20× or LUMPlanFL 40×, 60×; Olympus) and illuminated at 495 nm. Fluorescence was captured through a barrier filter above 515 nm, and images were obtained every 47–100 ms (frame interval) with an exposure time of 30–70 ms using a microphotoluminescence measurement system (AQUACOSMOS; Hamamatsu Photonics). Relative amplitudes of Ca^{2+} transients were expressed as $\Delta F_t/F_0 = (F_t - F_0)/F_0$, where F_t is the fluorescence generated by an event and baseline F_0 is the basal fluorescence.

To identify NG2(+) mural cells, DsRed fluorescence was excited at 515 nm, and emission was captured through a barrier filter above 575 nm.

The diameter of different microvasculature segments was measured manually by defining the boundaries of the

blood vessels in terms of their Cal-520 fluorescence on video images displayed by frame-by-frame playback. The major axis of cell bodies of five mural cells in each blood vessel segments were also measured and the averaged values were expressed as the soma length.

Intracellular recordings

The lamina propria preparations taken from non-carrier sibling or C57BL/6J mice were used for intracellular recording. Preparations were pinned out on a Sylgard plate at the bottom of the recording chamber mounted on the stage of an inverted microscope. Preparations were superfused with warmed (36°C) PSS at a constant flow rate (2 mL min^{-1}) and equilibrated for 90 min. Vascular mural cells were impaled with glass capillary microelectrodes, filled with 1 m KCl (tip resistance, 120–250 MΩ). Membrane potential changes were recorded using a high input impedance amplifier (Axoclamp-2B; Axon Instruments, Inc., Foster City, CA, USA) and displayed on a cathode-ray oscilloscope (SS-5702; Iwatsu, Tokyo, Japan). After low-pass filtering (cut-off frequency, 1 kHz), membrane potential changes were digitized using a Digidata 1322 interface (Axon Instruments, Inc.) and stored on a personal computer for later analysis.

Immunohistochemistry

The bladder was pinned flat in PBS at 4°C, and the muscle layer was removed using sharp tweezers and microscissors under a dissection microscope to make a mucosal preparation. A preparation that had been pinned flat was fixed with 4% paraformaldehyde in 0.1 M phosphate buffer (pH 7.3) for 15–30 min [3 h only for tyrosine hydroxylase (TH) immunohistochemistry] at 4°C, whereas tissue used for desmin immunostaining was fixed in acetone for 10 min at 4°C. After washing in PBS, the urothelium was removed only when mucosal preparation was used to immunostain for desmin, TH or α-SMA.

Detailed information of immunohistochemical protocol such as the blocking procedure or antibody dilution has been provided previously (Mitsui and Hashitani, 2013). Tissues were incubated with one or two primary antibodies overnight or for 2 days at 4°C or incubated with biotinylated swine anti-rabbit IgG antibody (dilution 1:300; Dako, Glostrup, Denmark) for 30 min only when rabbit primary antibody was used. The tissues were then incubated with a secondary antibody and/or Alexa488-conjugated streptavidin (10 μg mL^{-1}; Molecular Probes, Eugene, OR, USA) for 2 h.

Antibodies used were armenian hamster antibody for CD31 (dilution 1:200; Merck Millipore-Chemicon, Billerica, MA, USA), rabbit antibody for desmin (dilution 1:100; Abcam, Cambridge, UK), mouse antibody for endothelial nitric oxide synthase (eNOS) (dilution 1:400; BD Transduction Laboratories, Franklin Lakes, NJ, USA), rabbit antibody for TH (dilution 1:1000; Merck Millipore-Chemicon), mouse antibody for α-SMA (dilution 1:1000; clone 1A4; Sigma), Alexa488-conjugated goat anti-armenian hamster IgG antibody (7 μg mL^{-1}; Jackson Immunoresearch Laboratories, West Grove, PA, USA), Cy3-conjugated goat anti-mouse IgG antibody (2.5 μg mL^{-1}; Merck Millipore-Chemicon) and Alexa488-conjugated donkey anti-mouse IgG antibody (10 μg mL^{-1}; Abcam). Specimens were observed using a confocal laser scanning microscope (LSM 5 PASCAL; Carl Zeiss, Oberkochen, Germany).

Solutions

The composition of PSS was (in mM): 137.5 Na^+, 5.9 K^+, 2.5 Ca^{2+}, 1.2 Mg^{2+}, 15.5 HCO_3^-, 1.2 $H_2PO_4^-$, 134 Cl^- and 11.5 glucose. The pH of PSS was 7.2 when bubbled with 95% O_2 and 5% CO_2, and the measured pH of the organ bath solution was ~7.4. In a set of experiments, PSS was bubbled with 95% N_2 and 5% CO_2 to examine the effects of lowering oxygen concentrations on spontaneous Ca^{2+} transients.

The drugs used were Bay K 8644, caffeine, carbenoxolone, cyclopiazonic acid (CPA), 4,4′-di-isothiocyanato-2,2′-stilbenedisulphonic salt (DIDS), nicardipine, nickel chloride, nifedipine, niflumic acid and tetracaine (Sigma). Carbenoxolone and nickel chloride were dissolved in distilled water; Bay K 8644, CPA, nicardipine and tetracaine dissolved in dimethyl sulphoxide; and nifedipine and niflumic acid were dissolved in absolute ethanol. DIDS was directly dissolved in PSS immediately before use. The final concentration of the solvents above in the PSS did not exceed 1:1000.

Calculations and statistical analysis

The parameters of spontaneous Ca^{2+} transients measured were: the peak amplitude ($\Delta F_t/F_0$) measured as the value from the basal Ca^{2+} level to the peak of Ca^{2+} transients; half-width (s), measured as the time between 50% peak amplitude on the rising and falling phases; and frequency (min^{-1}) calculated as an average for over 5 min.

The parameters of electrical slow waves measured were: resting membrane potential (RMP) (mV); peak amplitude (mV), measured as the value from the RMP to the peak of events; half-width (s), measured as the time between 50% peak amplitude on the rising and falling phases; and frequency (min^{-1}), which was calculated as an average for over 3–5 min of recordings.

Measured values were expressed as the mean ± SD (where n is number of preparations as well as animals, unless otherwise specified). Statistical significance was tested using a paired t test. $P < 0.05$ was considered statistically significant.

The synchrony of Ca^{2+} transients amongst pericytes was analysed using the cross-correlation function of Clampfit, version 10.3 (Molecular Devices) as described previously.

Results

Morphological characteristics of mural cells in the suburothelial microvasculature network

In the bladder suburothelium of NG2-DsRed mice, the NG2-DsRed fluorescence of arteriolar SMCs and pericytes in branched PCAs and capillaries form an extensive tree-like network as visualized in Fig. 1*A*. The extensive network of NG2(+) pericyte-covered capillaries was located just beneath the urothelium (Fig. 1*B*), whereas the NG2(+) SMC or pericyte-covered arteriolar tree branching into capillaries was distributed in the lamina propria facing the detrusor smooth muscle layer (Fig. 1*C*). Staining of endothelium with CD31 visualized the whole microvasculature network (Fig. 1*D* and *E*), including NG2(–) pericyte-covered venules. Arteriolar SMCs expressed NG2-DsRed fluorescence, whereas no NG2-DsRed fluorescence was detected in pericyte-covered venules running in parallel. Capillary pericytes also expressed NG2-DsRed fluorescence, and pericytes in PCVs showed a faint NG2-DsRed signal.

At higher magnification, pericytes in PCAs had a typical 'bump-on-a-log' appearance with an NG2(+) oval cell body extending circumferentially-arranged processes and were also densely lined along the PCA axis (Fig. 1*F*). Desmin staining clearly revealed the stellate shaped morphology of NG2(–) pericytes in venules and NG2(+) pericytes in PCVs, as well as NG2(+) arteriolar SMCs (Fig. 1*G*). Capillary pericytes also had a bump-on-a-log appearance with an NG2(+) oval cell body but extended bipolar longitudinal processes running along the axis of capillaries that were visualized by eNOS staining of the endothelium (Fig. 1*H*).

These morphological characteristics of the mural cells in different microvascular segments are similar to those in the fluorescence labelled ureteric microvascular networks (Borysova *et al.* 2013) or mammary gland as identified by scanning electron microscopy (Fujiwara & Uehara, 1984). Thus, different segments of the microvasculature network could be identified by the morphology and NG2-DsRed expression of the mural cells.

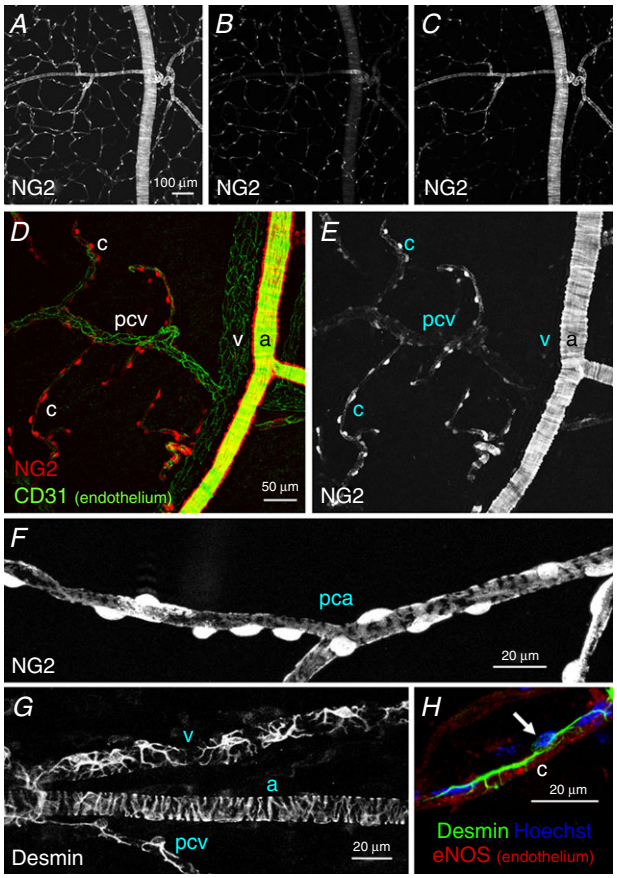

Figure 1. Morphological characteristics of mural cells in the microvasculature of bladder suburothelium
In a non-fixed mucosal preparation of NG2-DsRed mouse bladder, the DsRed fluorescence signal revealed the NG2-expressing mural cells in the microvascular network (*A*). A single plane image of the same area showed an extensive network of capillary pericytes just beneath the urothelium (*B*), whereas another single plane image visualized arteriolar tree branching capillaries in the outermost part of the lamina propria (*C*). In another lamina propria preparation processed for immunohistochemistry against the endothelial marker CD31, arteriolar smooth muscle cells expressed a strong NG2 signal (a), whereas no fluorescence was detected in venular pericytes (v) (*D* and *E*). Capillary pericytes (c) also expressed a strong NG2 signal, whereas pericytes in the postcapillary venule (pcv) showed faint NG2 signals (*D* and *E*). In a different lamina propria preparation, pericytes in the precapillary arteriole (pca) had an oval cell body expressing a strong NG2 signal and extended circumferentially-arranged processes with weaker NG2 signals (*F*). The stellate shaped morphology of pericytes in a venule (v) and a postcapillary venule (pcv) were revealed by desmin immunohistochemistry, whereas circumferentially-arranged processes were evident in the arteriole (a) (*G*). A capillary pericyte and endothelium (c) were visualized by their immunoreactivity for desmin (green) and eNOS (red), respectively (*H*). Nuclear staining with Hoechst (blue) indicated the pericyte cell body (arrow) extending longitudinally-oriented bipolar long processes. The scale bar in (*A*) also refers to (*B*) and (*C*), and that in (*D*) also refers to (*E*). [Colour figure can be viewed at wileyonlinelibrary.com]

Properties of spontaneous Ca^{2+} transients of mural cells in different microvasculature segments

Ca^{2+} dynamics of the mural cells were visualized *in situ* within lamina propria preparations in which the morphology and NG2 expression of the mural cells in different microvascular segments were observed simultaneously. Arterioles covered by circumferentially-arranged NG2(+) SMCs (Fig. 2*A* and *B*) branched into PCA where NG (+) pericytes were densely distributed (Fig. 2*A*, *C* and *F*). PCAs continued into capillaries where NG2(+) pericytes that had an oval shaped cell body with extending bipolar longitudinal processes (Fig. 2*G*) were more sparsely distributed (Fig. 2*A* and *D*). Pericytes in PCVs typically had short oval shaped cell bodies that expressed a faint NG2-DsRed fluorescence (Fig. 2*E*), although some PCV pericytes expressed brighter NG2-DsRed fluorescence (Fig. 2*F*). Morphological characteristics of pericytes in different microvascular segments are summarized in Fig. 2*H* and *I*. The diameter of capillaries is significantly smaller compared to PCAs or PCVs, whereas capillary pericytes have a larger soma length than pericytes in PCAs or PCVs.

NG2(+) pericytes in PCA developed synchronous spontaneous Ca^{2+} transients (Fig. 3*A* and *E*; see also Supporting information, Video S1), whereas NG2(+) pericytes in capillary exhibited nearly-synchronous spontaneous Ca^{2+} transients (Fig. 3*B* and *F*; see also Supporting information, Video S2). Within a capillary network, spontaneous Ca^{2+} transients in NG2(+) capillary pericytes propagated from one after another with an interpericyte distance of ~50 μm (Supporting information, Video S3). Within a PCA-capillary tree, spontaneous Ca^{2+} transients in NG2(+) capillary pericytes spread into the 'stem' PCA triggered

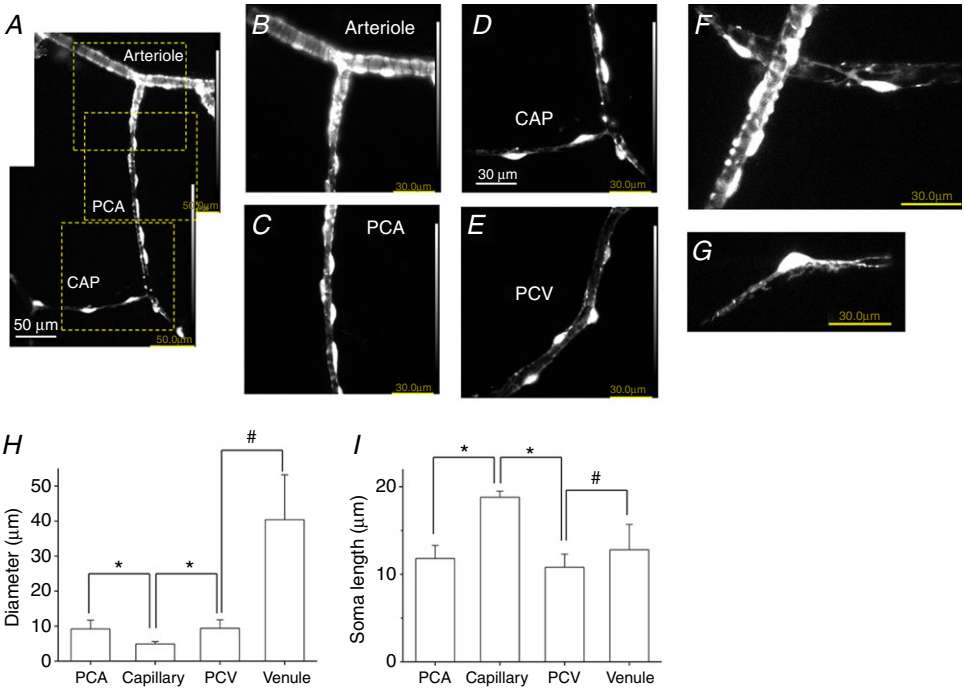

Figure 2. Morphological characteristics of mural cells in the microvasculature network for Ca^{2+} imaging
In a lamina propria preparation of NG2-DsRed mouse bladder used for Ca^{2+} imaging, an arteriole covered by circumferentially-arranged NG2(+) SMCs branched into a PCA where NG2(+) pericytes lined along the boundaries of the PCA wall (*A*). The PCA continued to a capillary (CAP) where NG2(+) pericytes were more sparsely distributed (*A*). An expanded image of the top dotted square in (*A*) revealed circumferentially-arranged NG2(+) arteriolar SMCs (*B*). An expanded image of the middle dotted square in (*A*) showed NG2(+) PCA pericytes with an oval shaped cell body extending circumferentially-oriented processes (*C*). An expanded image of the bottom dotted square in (*A*) showed NG2(+) CAP pericytes with an oval shaped cell body extending bipolar longitudinal processes (*D*). Pericytes in PCV had a short oval cell body that expressed a faint NG2 fluorescence (*E*). Note that luminance was increased for clarity. In another lamina propria preparation, NG2(+) pericytes extended circumferentially-oriented processes wrapped around PCA, whereas stellate-shaped NG2(+) pericytes were distributed in PCV (*F*). A capillary pericyte expressed strong NG2 fluorescence in the cell body and extended NG2(+) bipolar processes (*G*). Microvascular diameter (*H*) and soma length of pericytes (*I*) in different microvascular segments are summarized. Data are the mean ± SD. NS, not significantly different. *Significantly different from the values of capillary (unpaired Student's *t* test, $P < 0.05$). #Significantly different between the values of PCV and venule (unpaired Student's *t* test, $P < 0.05$). [Colour figure can be viewed at wileyonlinelibrary.com]

nearly-synchronous Ca^{2+} transients in not only NG2(+) PCA pericytes, but also NG2(+) pericytes in a branched capillary (Supporting information, Video S4). At the junction of PCA and capillary, Ca^{2+} transients in the NG2(+) capillary pericytes triggered Ca^{2+} transients in NG2(+) PCA pericytes and vice versa. As a result, NG2(+) pericytes in the connected PCA and capillaries generated Ca^{2+} transients at the same frequency, although any single capillary did not act as a constant driver.

NG2(+) pericytes in PCVs developed propagated spontaneous Ca^{2+} transients (Fig. 3*C* and *G*; see also Supporting information, Video S5). NG2(–) pericytes in venules also exhibited propagated spontaneous Ca^{2+} transients (Fig. 3*D* and *H*; see also Supporting information, Video S6) that had characteristics similar to those of venular Ca^{2+} transients of BALB/c mice bladder suburothelium (Hashitani *et al.* 2012). Consistent with a previous study (Hashitani *et al.* 2012), NG2(+) SMCs in arterioles remained quiescent (Fig. 3*H*; see also Supporting information, Video S6), although spontaneous Ca^{2+} transients were frequently seen presumably in endothelial cells. At the junction of PCV and venules, Ca^{2+} transients in NG2(+) PCV pericytes triggered Ca^{2+} transients in NG2(–) venular pericytes and vice versa (Supporting information, Video S7). Thus, pericytes in connected PCV and venules generated Ca^{2+} transients at the same

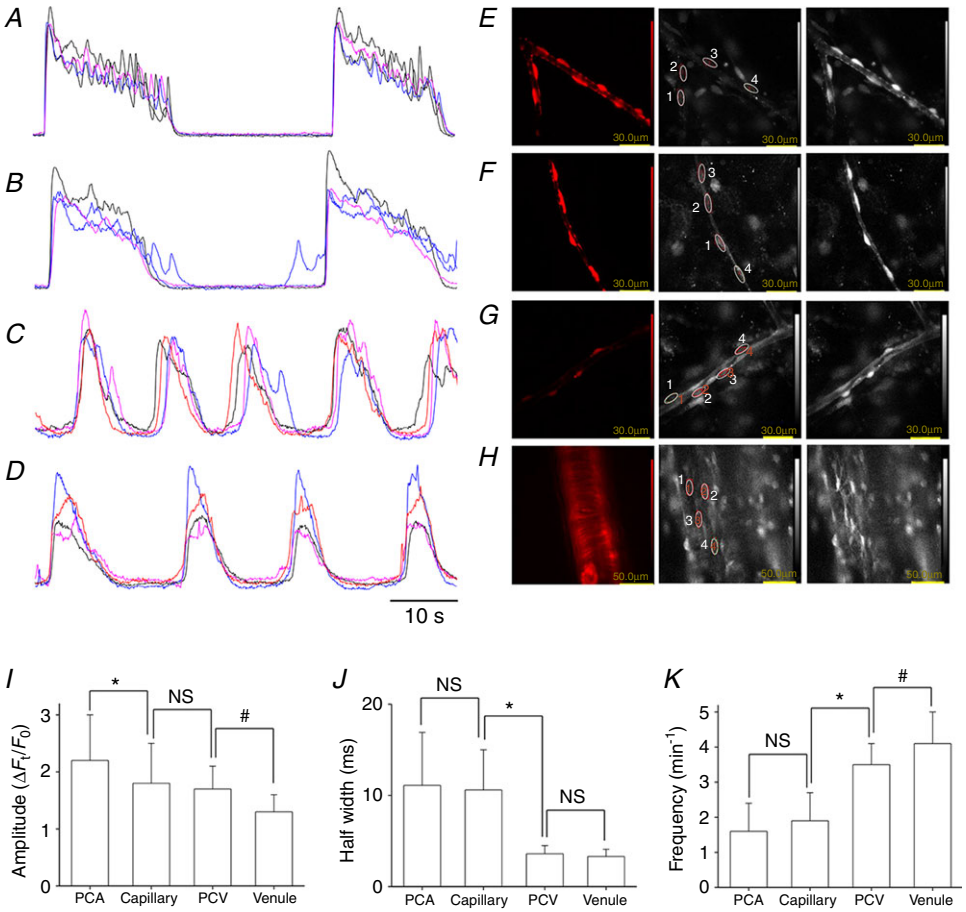

Figure 3. Spontaneous Ca^{2+} transients in different microvascular segments
In a PCA of NG2-DsRed mouse bladder, pericytes expressing a strong DsRed florescence developed synchronous spontaneous Ca^{2+} transients that lasted ~20 s (*A*). In a capillary, NG2/DsRed(+) pericytes developed nearly-synchronous spontaneous Ca^{2+} transients (*B*). In a PCV, pericytes expressing a faint DsRed fluorescence generated propagated spontaneous Ca^{2+} transients that lasted ~10 s (*C*). In a suburothelial venule, NG2(–) pericytes generated propagated spontaneous Ca^{2+} transients (*D*). The time scale bar refers to (*A*) to (*D*). Images of NG2 DsRed fluorescence (left) and Cal520 flourescence (middle, resting; right, Ca^{2+} transients) in pericytes of PCA (*E*), capillary (*F*), PCV (*G*) and venule (*H*). Note that NG2(–) venular pericytes but not NG2(+) arteriolar SMCs generated spontaneous Ca^{2+} transients (*H*). Amplitude (*I*), half-width (*J*) and frequency (*K*) of spontaneous Ca^{2+} transients in pericytes of different microvascular segments are summarized. Data are the mean ± SD. NS, Not significantly different. *Significantly different from the values of capillary pericytes (unpaired Student's *t* test, $P < 0.05$). #Significantly different between the values of PCV and venular pericytes (unpaired Student's *t* test, $P < 0.05$). [Colour figure can be viewed at wileyonlinelibrary.com]

frequency, although any single PCV did not constantly drive the connected venules. Parameters of spontaneous Ca^{2+} transients in pericytes of different microvascular segments are summarized in Fig. 3*I–K*. Spontaneous Ca^{2+} transients in pericytes of capillaries/PCAs were generated at a lower frequency than pericytes in PCVs/venules, whereas their half-with was longer than pericytes in PCVs/venules.

To determine whether the spontaneous Ca^{2+} transients in pericytes of the suburothelial microvasculature might be induced by a high oxygen concentration in the perfusate, a separate set of experiments was carried out using PSS bubbled with 95% N_2 and 5% CO_2. Pericytes in PCAs, capillaries, PCVs and venules generated spontaneous Ca^{2+} transients, and their parameters were not significantly different from those measured in the preparations superfused by PSS bubbled with 95% O_2 and 5% CO_2 (Table 1).

Spontaneous Ca^{2+} transients in NG2(+) pericytes in PCAs were associated with a ∼15 % reduction in the diameter of PCAs (from 9.7 ± 3.1 μm to 8.2 ± 2.2 μm, $n = 42$), whereas Ca^{2+} transients in NG2(+) pericytes in capillaries did not result in a reduction of capillary diameter. Spontaneous Ca^{2+} transients in NG2(+) pericytes in PCVs were not associated with an evident reduction in the PCV diameter, whereas Ca^{2+} transients in NG2(–) venular pericytes resulted in a ∼25% reduction of the venular diameter (from 42.3 ± 13.1 μm to 32.6 ± 12.3 μm, $n = 35$). These values of spontaneous venular constrictions were not very different from those reported in the suburothelial venules of BALB/c mice (Hashitani *et al.* 2012) or rat (Hashitani *et al.* 2011) bladders.

Consistent with the contractile properties in the different microvascular units, α-SMA was strongly expressed in NG2(+) pericytes in PCAs (Fig. 4*A–C*) or NG2(–) pericytes in venules (Fig. 4*G–I*), whereas no α-SMA expression was evident NG2(+) capillary pericytes (Fig. 4*A–F*). NG2(+) pericytes in PCVs with a diameter of ∼20 μm expressed α-SMA (Fig. 4*D–F*), although their α-SMA expression was largely diminished in PCVs with a diameter of less than 10 μm (Fig. 4*G–I*).

Roles of LVDCCs in pericyte Ca^{2+} transients of different microvascular segments

Because LVDCCs play a fundamental role in maintaining the synchrony of spontaneous Ca^{2+} transients amongst mural cells in many vascular beds including suburothelial venules (Hashitani *et al.* 2011; Hashitani *et al*, 2012), the effects of LVDCC blockade with nifedipine on Ca^{2+} transients in different microvascular segments were compared.

In PCAs, nifedipine (3 μM, $n = 16$ or 10 μM, $n = 4$) abolished pericyte Ca^{2+} transients ($n = 8$) (Fig. 5*A*) or disrupted their synchrony ($n = 12$) (Fig. 5*B* and *C*). Subsequent BayK 8644 (1 μM), a LVDCC activator, recovered spontaneous Ca^{2+} transients in the arrested pericytes of PCA ($n = 3$) or restored their synchrony ($n = 4$) (Fig. 5*D*). Cross-correlation analysis applied to PCA pericyte Ca^{2+} transients demonstrated that the prominent peak near time zero seen in control (Fig. 5*E*) was greatly suppressed by nifedipine (Fig. 5*F*) in a manner reversed by BayK 8644 ($n = 4$) (Fig. 5*G*). In 12 PCAs in which nifedipine (3 or 10 μM) disrupted the synchrony of spontaneous Ca^{2+} transients, the amplitude and the half-width of pericyte Ca^{2+} transients were reduced but their frequency was increased (Fig. 5*M–O*).

In capillaries, nifedipine (3 μM, $n = 10$ or 10 μM, n = 5) shortened spontaneous pericyte Ca^{2+} transients but failed to disrupt their synchrony (Fig. 5*H* and *I*). Cross-correlation analysis of Ca^{2+} transients amongst pericytes demonstrated that the prominent peak near time zero seen in control (Fig. 5*J*) was not diminished by nifedipine ($n = 10$ (Fig. 5*K*). In 15 capillaries, nifedipine (3 or 10 μM) reduced the amplitude and the half-width of pericyte Ca^{2+} transients but increased their frequency (Fig. 5*M–O*). Thus, LVDCCs appear to play a critical role in the generation or synchrony of spontaneous Ca^{2+} transients in PCA pericytes but not capillary pericytes.

Nifedipine (1 μM) suppressed Ca^{2+} transients in PCVs and disrupted their synchrony ($n = 5$) (Fig. 5*L*) in a manner reversed by Bay K8644 (1 μM). In five PCVs

Table 1. Parameters of spontaneous Ca^{2+} transients in pericytes of different microvascular segments measured with 95% N_2 + 5% CO_2

Segment	Amplitude ($\Delta F_t/F_0$)	Half-width (s)	Frequency (min^{-1})
PCAs ($n = 5$)	2.28 ± 0.44 NS	13.2 ± 4.7 NS	1.54 ± 0.37 NS
Capillaries ($n = 5$)	1.99 ± 0.52 NS	12.9 ± 4.4 NS	1.74 ± 0.36 NS
PCVs ($n = 6$)	1.76 ± 0.28 NS	4.28 ± 0.85 NS	3.45 ± 0.21 NS
Venules ($n = 5$)	1.29 ± 0.28 NS	3.56 ± 0.61 NS	4.0 ± 1.26 NS

Data shown are the mean ± SD. NS, not significantly different from the values measured with 95% O_2 + 5% CO_2 ($P < 0.05$).

that had been exposed to nifedipine, the amplitude, half-width and frequency of Ca^{2+} transients were reduced (Fig. 5*M–O*).

Because the synchrony of LVDCC independent spontaneous Ca^{2+} transients in myenteric capillary pericytes of the guinea-pig stomach was disrupted by the blockade of TVDCCs (Hashitani *et al.*, 2015), the effects of nickel ions (Ni^{2+}), a known blocker of TVDCCs, on the nifedipine-resistant spontaneous Ca^{2+} transients in capillary pericytes were also examined.

In preparations that had been pretreated with nifedipine (3 μM) in which capillary pericytes continued to generate synchronous spontaneous Ca^{2+} transients, subsequent application of $NiCl_2$ (100 μM) failed to disrupt their synchrony ($n = 5$). $NiCl_2$ (100 μM) did not change the amplitude ($2.3 \pm 0.6\ \Delta F_t/F_0$ in control, $2.2 \pm 0.6\ \Delta F_t/F_0$ in Ni^{2+}, $P > 0.05$), half-width (from 4.8 ± 2.4 s in control, 4.9 ± 2.1 s in Ni^{2+}, $P > 0.05$) or the frequency ($2.1 \pm 0.7\ min^{-1}$ in control, $2.1 \pm 0.6\ min^{-1}$ in Ni^{2+}, $P > 0.05$) of the spontaneous Ca^{2+} transients in capillary pericytes.

Roles of gap junctions in generating pericyte Ca^{2+} transients of different microvascular segments

More pronounced inhibitory effects of LVDCC blockade on pericyte Ca^{2+} transients in PCA and PCVs than those of capillary pericyte may indicate that pericyte Ca^{2+} transients in PCAs and PCVs are driven by capillary pericytes. Thus, the effects of carbenoxolone, a gap junction blocker, on pericyte Ca^{2+} transients in different microvascular segments were examined.

Carbenoxolone (10 μM) invariably abolished spontaneous Ca^{2+} transients in PCA pericytes ($n = 15$) (Fig. 6*A*), whereas it disrupted or diminished the synchrony of pericyte Ca^{2+} transients in capillaries ($n = 12$) (Fig. 6*B*). At the junction of PCAs and

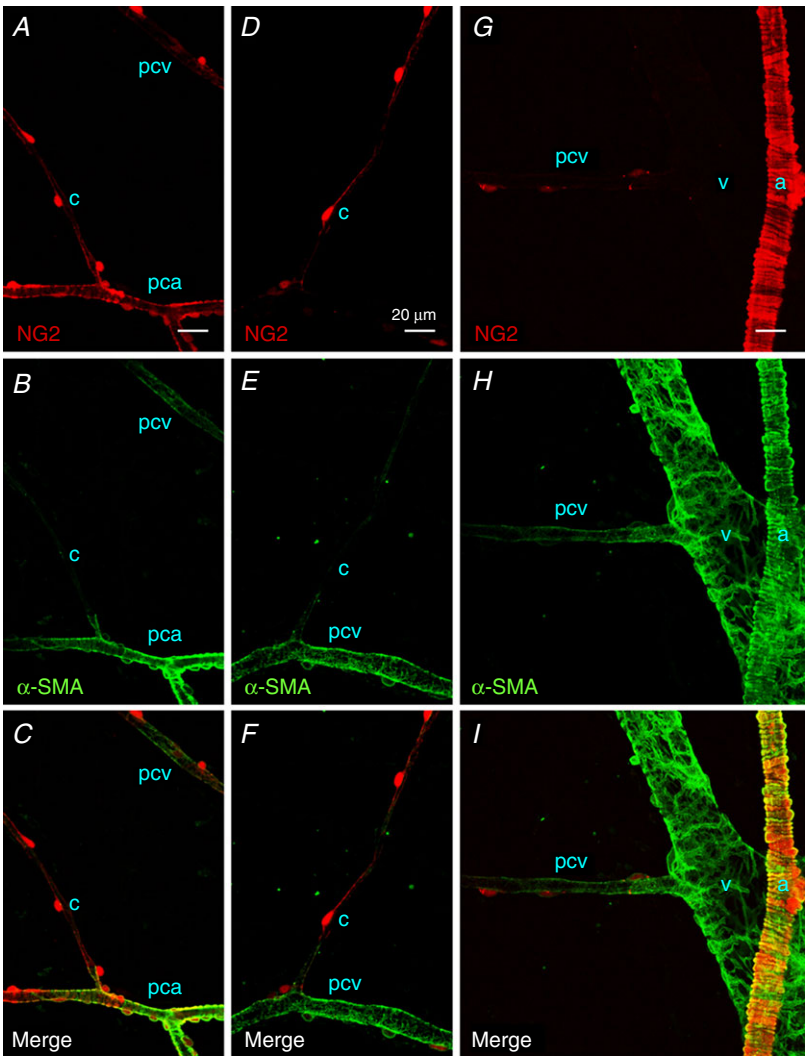

Figure 4. Immunoreactivity for α-SMA in different segments of suburothelial microvessels of NG2 DsRed mouse bladder
Pericytes in a PCA expressed a red NG2 signal (pca), as well as α-SMA immunoreactivity (green), whereas the NG2-expressing pericytes in a capillary (c) branching from the PCA were α-SMA-negative (*A–C*). In the same micrographs, NG2(+) pericytes in a postcapillary venule (pcv) expressed faint α-SMA immunoreactivity. NG2(+) pericytes in a postcapillary venule (pcv) but not those in a connecting capillary (c) exhibited α-SMA immunoreactivity (*D–F*). Pericytes in a larger venule without NG2 signal (v) showed strong α-SMA-immunoreactivity, and a connecting postcapillary venule with faint NG2 signal (pcv) exhibited weaker α-SMA-immunoreactivity (*G–I*). Smooth muscle cells in an arteriole (a) expressing a bright red NG2 signal showed strong α-SMA immunoreactivity. The scale bar in (*A*) = 20 μm also refers to (*B*) to (*I*). [Colour figure can be viewed at wileyonlinelibrary.com]

capillaries, carbenoxolone (10 μM) abolished PCA Ca^{2+} transients, whereas it left capillary Ca^{2+} transients ($n = 4$) (Supporting information, Video S8 and S9), supporting the notion that capillary pericytes drive PCA pericytes. Cross-correlation analysis applied to capillary pericyte Ca^{2+} transients demonstrated that the prominent peak near time zero seen in control (Fig. 6*C*) was diminished by carbenoxolone ($n = 5$) (Fig. 6*D*). In 12 capillaries that had been exposed to carbenoxolone, the amplitude and the half-width of pericyte Ca^{2+} transients were reduced, although their frequency was increased (Fig. 6*I–K*).

In PCVs, carbenoxolone (10 μM) abolished pericyte Ca^{2+} transients ($n = 8$) or disrupted their synchrony ($n = 5$) (Fig. 6*E*). Cross-correlation analysis applied to pericyte Ca^{2+} transients in PCVs demonstrated that the prominent peak near time zero was (Fig. 6*F*) greatly suppressed by carbenoxolone ($n = 5$) (Fig. 6*G*). In five PCVs that had been exposed to carbenoxolone, amplitude, half-width and frequency of pericyte Ca^{2+} transients were all reduced (Fig. 6*I–K*).

In venules, carbenoxolone (10 μM) invariably prevented the generation of pericyte Ca^{2+} transients ($n = 6$) (Fig. 6*H*).

Roles of Ca^{2+}-activated chloride channels in generating pericyte Ca^{2+} transients of different microvascular segments

To further explore the mechanism underlying inter-segmental transmission of pericyte Ca^{2+} transients, the effects of DIDS, a known blocker of Ca^{2+}-activated chloride channels (CaCCs), on pericyte Ca^{2+} transients in different microvascular segments were examined.

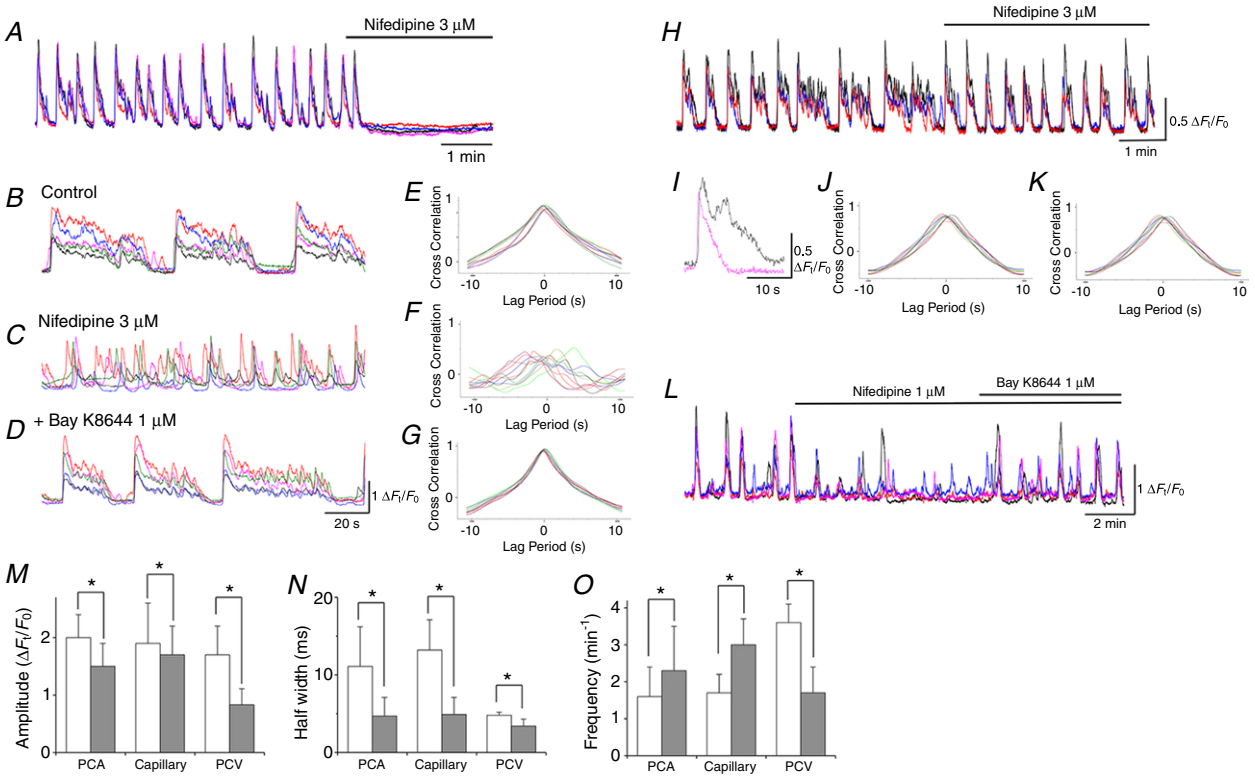

Figure 5. Role *of LVDCC* in maintaining the synchrony of pericyte Ca^{2+} transients in different microvascular segments

In a PCA, nifedipine (3 μM) abolished synchronous spontaneous Ca^{2+} transients in four pericytes (*A*). In a different PCA where five pericytes generated synchronous spontaneous Ca^{2+} transients (*B*), nifedipine (3 μM) disrupted their synchrony (*C*). Subsequent BayK8644 (1 μM) restored their synchrony (*D*). Cross-correlation analysis demonstrated prominent peak near time zero in control (*E*) and in BayK8644 (*G*) but not in nifedipine (*F*). In a capillary, three pericytes exhibited synchronous spontaneous Ca^{2+} transients (*H*). Nifedipine (3 μM) shortened the spontaneous Ca^{2+} transients (*I*) but did not disrupt their synchrony. Cross-correlation analysis demonstrated prominent peak near time zero in both control (*J*) and in nifedipine (*K*). In a PCV, nifedipine (1 μM) disrupted the synchrony of spontaneous Ca^{2+} transients amongst four pericytes (*L*). Subsequent BayK8644 (1 μM) restored their synchrony. Amplitude (*M*), half-width (*N*) and frequency (*O*) of spontaneous Ca^{2+} transients in pericytes of different microvascular segments are summarized. Data are the mean ± SD. *Significantly different from the control values (paired Student's *t* test, $P < 0.05$). [Colour figure can be viewed at wileyonlinelibrary.com]

DIDS (100 μM) invariably abolished spontaneous Ca^{2+} transients in pericytes of PCAs (n = 8) (Fig. 7*A*), whereas it disrupted the synchrony of Ca^{2+} transients in capillary pericytes (n = 10) (Fig. 7*B*). At the PCA-capillary junction, DIDS (100 μM) abolished PCA Ca^{2+} transients, at the same time as leaving the capillary Ca^{2+} transients (n = 4), suggesting that CaCC-dependent depolarizations generated in capillary pericytes are transmitted to PCA pericytes. Cross-correlation analysis applied to capillary pericyte Ca^{2+} transients demonstrated that the prominent peak near time zero seen in control (Fig. 7*C*) was diminished by DIDS (n = 6) (Fig. 7*D*). In 10 capillaries that had been exposed to DIDS, amplitude and half-width of pericyte Ca^{2+} transients were reduced, whereas their frequency was increased (Fig. 7*I–K*).

DIDS (100 μM) disrupted the synchrony of pericyte Ca^{2+} transients in PCVs (n = 6) (Fig. 7*E*). Cross-correlation analysis of pericyte Ca^{2+} transients in PCVs demonstrated that the prominent peak near time zero seen in control (Fig. 7*F*) was diminished by DIDS (n = 6) (Fig. 7*G*). In six PCVs that had been exposed to DIDS, amplitude, half-width and frequency of pericyte Ca^{2+} transients were reduced (Fig. 7*I–K*).

DIDS (100 μM) invariably prevented the generation of pericyte Ca^{2+} transients in venules (n = 10) (Fig. 7*H*).

Roles of sarco- and endoplasmic reticulum (SR/ER) Ca^{2+} handling in generating pericyte Ca^{2+} transients of different microvascular segments

Our previous studies demonstrated that spontaneous Ca^{2+} transients in venular pericytes of the bladder suburothelium arise from the cycles of spontaneous uptake and release of Ca^{2+} by SR/ER (Hashitani *et al.* 2011;

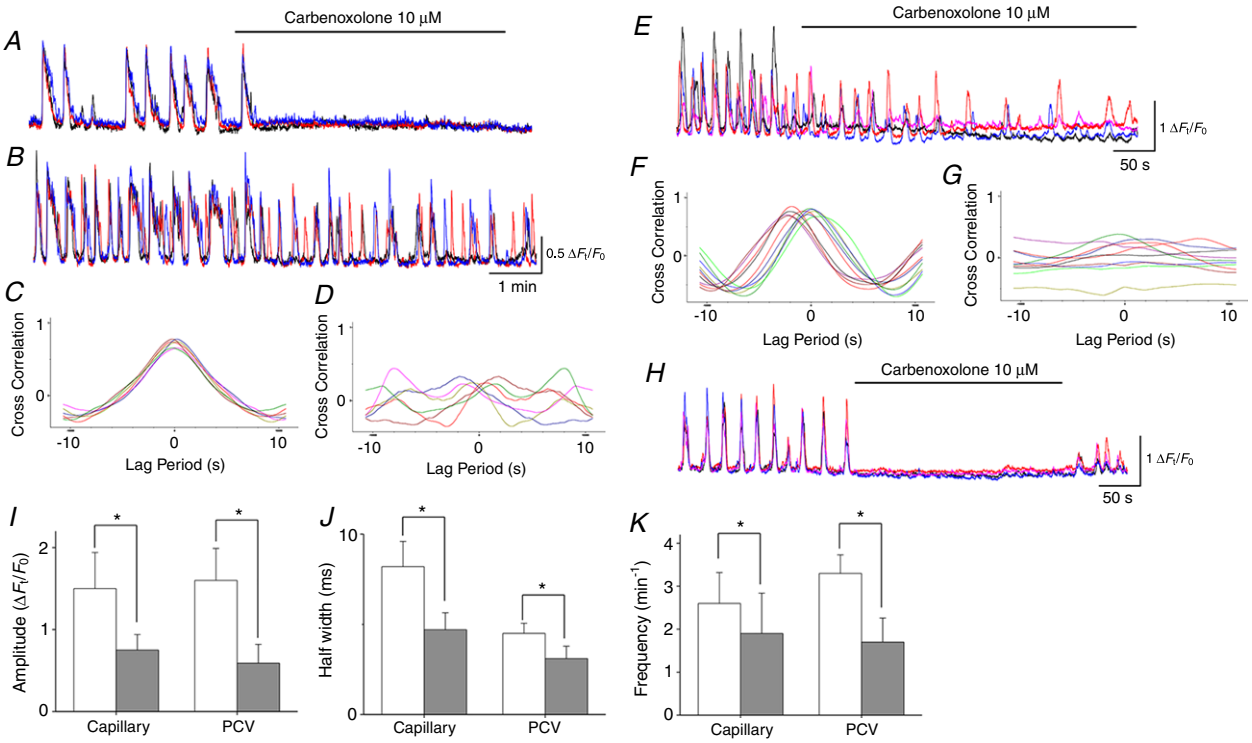

Figure 6. Role of gap junction in generating pericyte Ca^{2+} transients in different microvascular segments
In a PCA where three pericytes generated synchronous spontaneous Ca^{2+} transients, carbenoxolone (10 μM) prevented the generation of Ca^{2+} transients (*A*). Simultaneous recording from a connected capillary demonstrated that three pericytes generated synchronous spontaneous Ca^{2+} transients and carbenoxolone (10 μM) disrupted their synchrony (*B*). Cross-correlation analysis demonstrated prominent peak near time zero in both control (*C*) but not in carbenoxolone (*D*). In a PCV, carbenoxolone (10 μM) disrupted the synchrony of spontaneous Ca^{2+} transients amongst four pericytes (*E*). Cross-correlation analysis demonstrated that the prominent peak near time zero in control (*F*) but not in carbenoxolone (*G*). In a venule, carbenoxolone (10 μM) abolished synchronous spontaneous Ca^{2+} transients in four pericytes (*H*). Spontaneous Ca^{2+} transients were restored after washout of carbenoxolone. Amplitude (*I*), half-width (*J*) and frequency (*K*) of spontaneous Ca^{2+} transients in pericytes of capillary and PCV are summarized. Data are the mean ± SD. *Significantly different from the control values (paired Student's t test, $P < 0.05$). [Colour figure can be viewed at wileyonlinelibrary.com]

Hashitani *et al.* 2012). Therefore, the role of SR/ER Ca^{2+} handling in generating pericyte Ca^{2+} transients of other microvascular segments was examined.

In PCA, CPA (10 μM) abolished spontaneous Ca^{2+} transients in pericytes and increased the basal Ca^{2+} levels by 0.44 ± 0.18 $\Delta F_t/F_0$ (n = 8) (Fig. 8*A*), irrespective of the presence (n = 4) or absence (n = 4) of nifedipine. Caffeine (1 mM), which is known to stimulate ryanodine receptor-mediated Ca^{2+} release but inhibit IP_3 receptor-mediated Ca^{2+} release (Hirose *et al.* 1993), abolished (n = 11) (Fig. 8*B*) or inhibited (n = 2) pericyte Ca^{2+} transients in PCA. In the two PCAs, caffeine (1 mM) reduced the amplitude (from 2.0 ± 0.6 to 1.0 ± 0.6 $\Delta F_t/F_0$), half-with (from 14.1 ± 6.0 to 9.3 ± 3.5 s) and frequency (from 2.2 ± 0.5 to 0.8 ± 0.6 min^{-1}) of pericyte Ca^{2+} transients. Tetracaine (100 μM), a blocker of Ca^{2+}-induced Ca^{2+} release via ryanodine receptors, abolished (n = 6) (Fig. 8*C*) or inhibited (n = 5) pericyte Ca^{2+} transients in PCAs. In the five PCAs, tetracaine (100 μM) suppressed the amplitude (from 2.1 ± 0.7 to 1.3 ± 0.5 $\Delta F_t/F_0$, $P < 0.05$), half-width (from 8.4 ± 1.7 to 4.5 ± 1.1 s, $P < 0.05$) and frequency (from 1.9 ± 0.4 to 1.2 ± 0.5 min^{-1}, $P < 0.05$) of pericyte Ca^{2+} transients.

In capillaries, CPA (10 μM) prevented the generation of spontaneous Ca^{2+} transients in pericytes associated with a rise in the basal Ca^{2+} levels by 0.36 ± 0.1 $\Delta F_t/F_0$ (Fig. 8*D*), irrespective of the presence (n = 2) or absence (n = 3) of nifedipine. Caffeine (1 mM) abolished (n = 6) or inhibited (n = 3) pericyte Ca^{2+} transients in capillaries (Fig. 8*E*). In the three capillaries, caffeine (1 mM) reduced the amplitude (from 1.5 ± 0.3 to 0.6 ± 0.3 $\Delta F_t/F_0$, $P < 0.05$) and frequency (from 3.2 ± 0.2 to 1.6 ± 0.4 min^{-1}, $P < 0.05$) of the pericyte Ca^{2+} transients without affecting their half-with (from 5.4 ± 1.9 to 5.3 ± 1.7 s, $P > 0.05$). Tetracaine (100 μM) also abolished (n = 3) or inhibited (n = 4) spontaneous Ca^{2+} transients in capillary pericytes (Fig. 8*F*). In the four capillaries, tetracaine (100 μM) reduced the amplitude (from 1.5 ± 0.2 to 0.8 ± 0.2

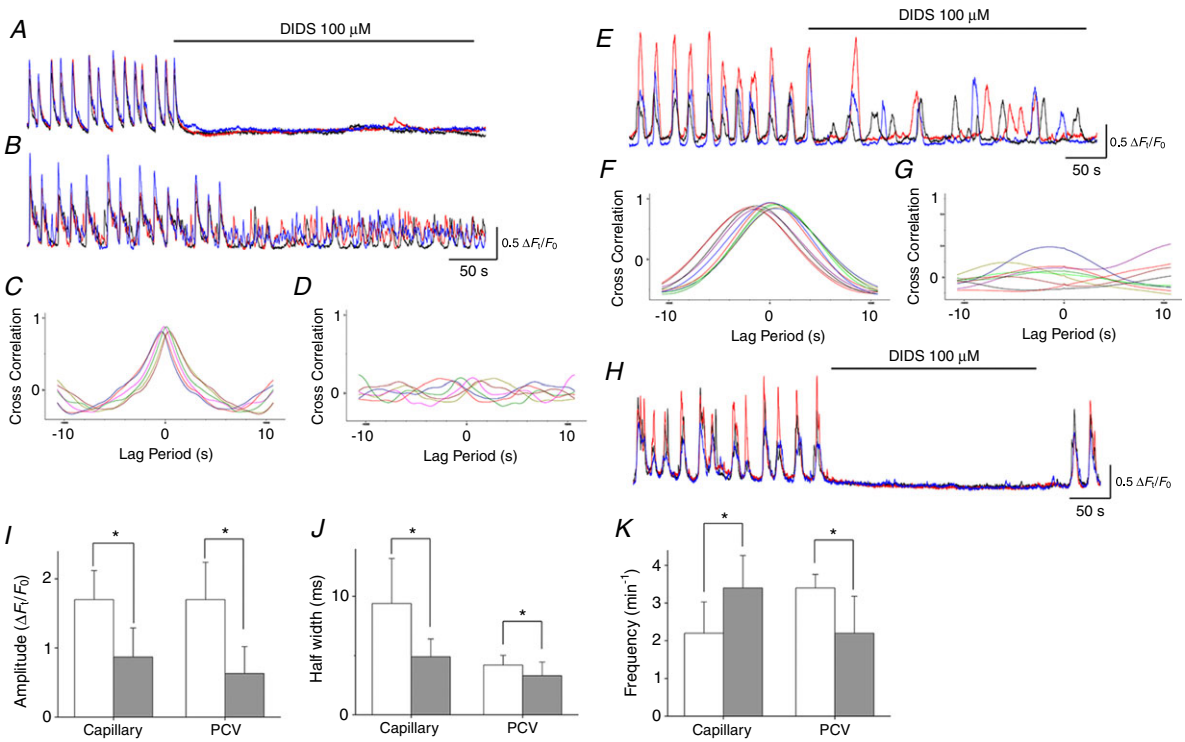

Figure 7. Role of CaCC in generating pericyte Ca^{2+} transients in different microvascular segments
In a PCA, DIDS (100 μM) prevented the generation of synchronous spontaneous Ca^{2+} transients in three pericytes (*A*). Simultaneous recording from three pericytes in a connected capillary showed synchronous spontaneous Ca^{2+} transient but DIDS (100 μM) suppressed the Ca^{2+} transients and disrupted their synchrony (*B*). Cross-correlation analysis demonstrated that the prominent peak near time zero in control (*C*) was largely suppressed by DIDS (*D*). In a PCV, DIDS (100 μM) disrupted the synchrony of spontaneous Ca^{2+} transients amongst three pericytes (*E*). Cross-correlation analysis showed that the prominent peak near time zero in control (*F*) was largely suppressed by DIDS (*G*). In a venule, DIDS (100 μM) prevented the generation of synchronous spontaneous Ca^{2+} transients in three pericytes (*H*). Spontaneous Ca^{2+} transients were restored after washout of carbenoxolone. Amplitude (*I*), half-width (*J*) and frequency (*K*) of spontaneous Ca^{2+} transients in pericytes of capillary and PCV are summarized. Data are the mean ± SD. *Significantly different from the control values (paired Student's *t* test, $P < 0.05$). [Colour figure can be viewed at wileyonlinelibrary.com]

$\Delta F_t/F_0$, $P < 0.05$) and frequency (from 2.9 ± 0.4 to 1.5 ± 0.8 min^{-1}, $P < 0.05$) of the pericyte Ca^{2+} transients without affecting their half-width (from 4.3 ± 1.0 to 4.0 ± 0.9 s, $P > 0.05$).

In PCV, pericyte Ca^{2+} transients were abolished by CPA (10 μM) associated with a rise in the basal Ca^{2+} level by 0.41 ± 0.13 $\Delta F_t/F_0$ ($n = 7$) (Fig. 8*G*). Caffeine (1 mM) also prevented the generation of PCV Ca^{2+} transients ($n = 8$) (Fig. 8*H*). Tetracaine (100 μM) abolished ($n = 4$) (Fig. 8*I*) or inhibited ($n = 3$) pericyte Ca^{2+} transients in PCVs. In the three PCVs, tetracaine (100 μM) reduced the amplitude (from 1.8 ± 0.4 to 0.32 ± 0.12 $\Delta F_t/F_0$, $P < 0.05$), half-width (from 3.8 ± 0.25 to 3.2 ± 0.36 s, $P < 0.05$) and frequency (from 3.6 ± 0.45 to 1.1 ± 0.25 min^{-1}, $P < 0.05$) of the pericyte Ca^{2+} transients.

Comparison of electrical properties of venular pericytes and arteriolar SMCs

Ca^{2+} imaging of the suburothelial microvasculature networks of NG2-DeRed mice revealed that pericytes in different microvascular segments developed spontaneous Ca^{2+} transients, whereas arteriolar SMCs remained quiescent. Thus, the electrical properties of pericyte-covered venules and SMC-covered arterioles were investigated.

In venules, pericytes had a resting membrane potential of –45 ± 1.8 mV. Venular pericytes exhibited slow waves that had amplitude of 17.7 ± 1.2 mV (peak values = –27 mV), half-width of 4.3 ± 0.2s (Fig. 9*A* and *B*) and frequency of 4.5 ± 0.3 min^{-1} ($n = 9$) (Fig. 9*A*, *B* and *E*).

Nicardipine (1 μM, $n = 4$), a blocker for LVDCC, depolarized the membrane by 7.4 ± 2.1 mV and prevented the generation of regularly generated slow waves (Fig. 9*A*). Expanding the timescale revealed that nicardipine prevented slow wave generation leaving spontaneous transient depolarizations (STDs) (Fig. 9*C*). STDs were suppressed by subsequent addition of niflumic acid (50 μM), a known blocker for CaCC, associated with a hyperpolarization of the membrane (7.5 ± 2.0 mV, $n = 4$) (Fig. 9*D*). Slow waves were also blocked by levcromakalim (100 μM), an ATP-sensitive K^+ channel opener, associated with a hyperpolarization of 18.3 ± 3.2 mV ($n = 4$) (Fig. 9*E*).

In arterioles, SMCs had a resting membrane potential of –70 ± 3.8 mV and remained electrically quiescent ($n = 8$). Ba^{2+} (1 mM), a known blocker of inward rectifier K^+

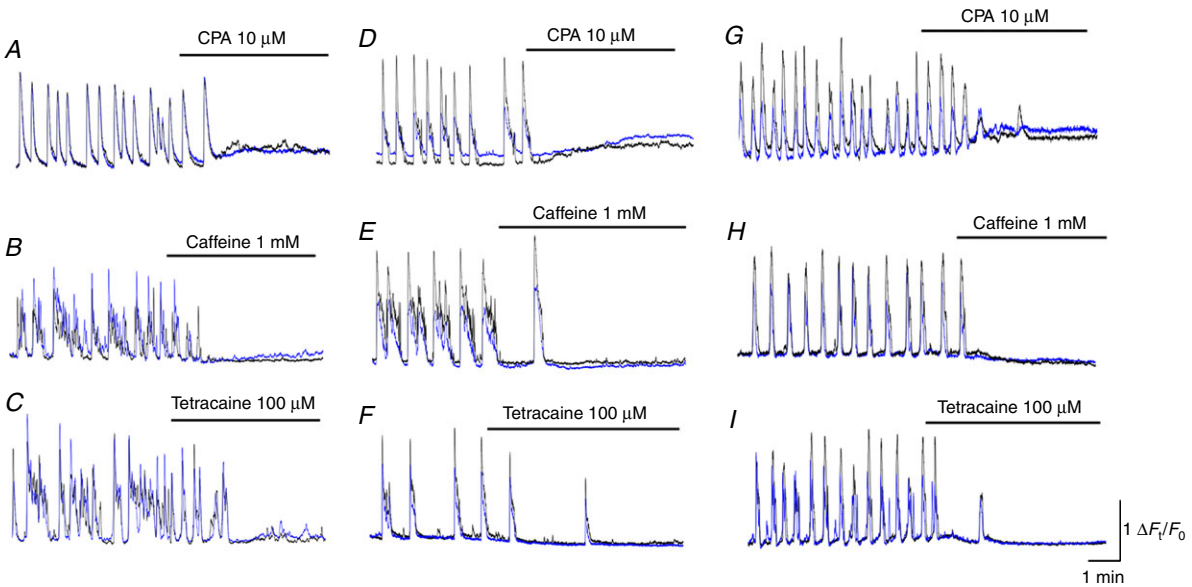

Figure 8. Role of intracellular Ca^{2+} stores in generating pericyte Ca^{2+} transients in different microvascular segments
In a PCA, CPA (10 μM) abolished spontaneous Ca^{2+} transients in pericytes and increased the basal Ca^{2+} level (*A*). In another PCA, caffeine (1 mM) prevented the generation of spontaneous Ca^{2+} transients in pericytes (*B*). In a different PCA, tetracaine (100 μM) abolished spontaneous Ca^{2+} transients in pericytes (*C*). In a capillary, CPA (10 μM) abolished spontaneous Ca^{2+} transients in pericytes associated with a rise in the basal Ca^{2+} level (*D*). In another capillary, caffeine (1 mM) prevented the generation of spontaneous Ca^{2+} transients in pericytes (*E*). In the same capillary, tetracaine (100 μM) abolished spontaneous Ca^{2+} transients in pericytes (*F*). In a PCV, CPA (10 μM) prevented the generation of spontaneous Ca^{2+} transients in pericytes associated with a rise in the basal Ca^{2+} level (*G*). In another PCV, caffeine (1 mM) abolished spontaneous Ca^{2+} transients in pericytes (*H*). In a different PCV, tetracaine blocked spontaneous Ca^{2+} transients in pericytes (*I*). [Colour figure can be viewed at wileyonlinelibrary.com]

channels, depolarized the membrane to –45 ± 3.8 mV (n = 5). Subsequent ACh (1 μM) hyperpolarized the membrane to –73 ± 3.8 mV (n = 5), indicating that the endothelium is intact and functional.

Nerve-evoked Ca^{2+} transients in arteriolar SMCs and venular pericytes

Responses to electrical field stimulation (EFS) (10 or 20 Hz, 1s, pulse width 50 μs) were examined in different microvascular units.

EFS triggered rapid Ca^{2+} transients in arteriolar SMCs, at the same time as inducing 'slow onset' Ca^{2+} transients in venular pericytes (Fig. 10*A*); Nerve-evoked Ca^{2+} transients in arterioles had a time to peak of 2.1 ± 0.16 s, an amplitude of 0.87 ± 0.38 $\Delta F_t/F_0$ and a half-width of 2.0 ± 0.16 s (n = 9). Nerve-evoked Ca^{2+} transients in venules had the time to peak of 4.6 ± 0.51 s, an amplitude of 1.5 ± 0.62 $\Delta F_t/F_0$ and a half-width of 4.8 ± 0.31 s (n = 7). Nerve-evoked Ca^{2+} transients in both arterioles and venules were blocked by guanethidine (10 μM). By contrast to relatively larger microvessels, nerve-evoked Ca^{2+} transients were hardly detected in pericyte of PCAs, capillaries or PCVs.

Consistent with the results of the EFS-induced responses, immunohistochemistry of TH, a sympathetic never maker, demonstrated varicose TH-positive nerve fibers running along SMC-containing arterioles and pericyte-covered venules (Fig. 10*B* and *C*) but not pericyte-covered microvascular PCAs, capillaries or PCVs (Fig. 10*D* and *E*).

Discussion

In the bladder suburothelium of NG2-DsRed mice, Ca^{2+} signals were visualized in mural cells in different segments of microvascular units that were identified by their morphology and NG2-DsRed fluorescence. Besides the NG2(–) venular pericytes that are known to develop synchronous spontaneous Ca^{2+} transients (Hashitani *et al.* 2012), NG2(+) pericytes in PCAs, capillaries and PCVs exhibited synchronous or propagated spontaneous Ca^{2+} transients, whereas NG2(+) arteriolar SMCs remained quiescent. Thus, the suburothelial microvascular appears to function as an integrated unit with the exception of the arterioles.

Morphological and functional characteristics in different microvascular segments

In the suburothelial layer facing the detrusor smooth muscle layer, arterioles branching into PCAs run in parallel to venules collecting PCVs. PCAs branching into

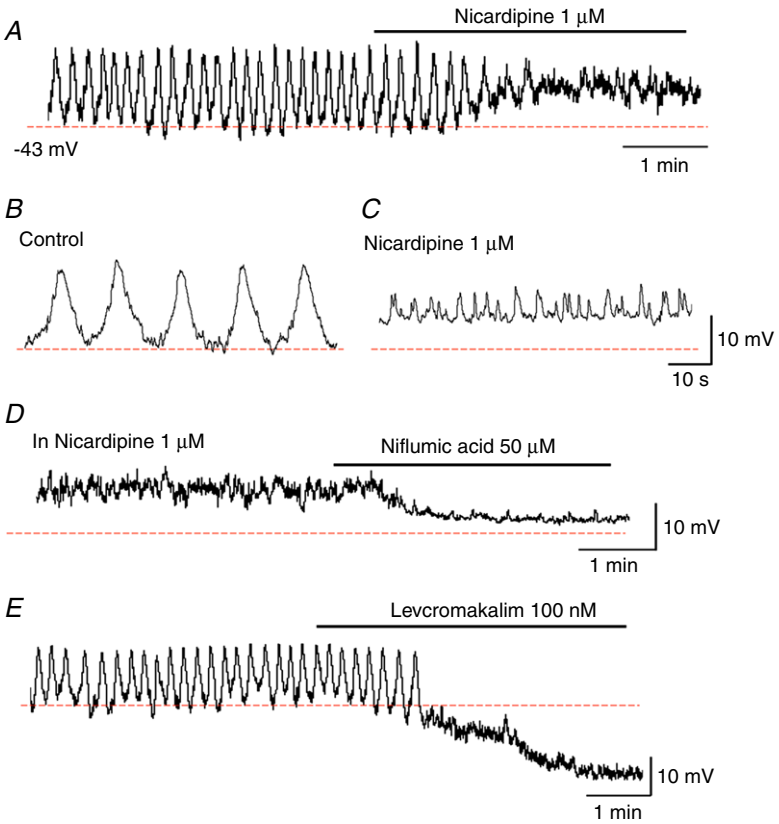

Figure 9. Electrical properties of venular pericytes
In a venule where pericytes periodically generated slow waves, nicardipine (1 μM) depolarized the membrane by ~10 mV and prevented the slow wave generation leaving STDs (*A*). The traces with an expanded time scale showed slow waves in control (*B*) and STDs in nicardipine (*C*). In the same venule, subsequent niflumic acid (1 μM) hyperpolarized the membrane by ~10 mV and abolished STDs (*D*). In another venule where slow waves were generated, levcromakalim (100 nM) hyperpolarized the membrane by ~15 mV and abolished slow waves (*E*). [Colour figure can be viewed at wileyonlinelibrary.com]

an extensive capillary network distributed just beneath the urothelium, suggesting that the capillary network functions to maintain the metabolic demands of the urothelium–sensory nerve complex that generates and conveys bladder sensations to the CNS (Birder and Andersson, 2013).

In the suburothelial layer of NG2-DeRed mice, different segments of the microvascular unit were readily identified by the morphology of the mural cells. Consistent with our previous immunohistochemical study in the fixed bladder suburothelium using NG2 antibody (Mitsui & Hashitani, 2013), stellate shaped pericytes enveloping venules did not express NG2-DeRed florescence. By contrast, pericytes in PCVs flowing into the venules had a 'bump-on-a-log' appearance, extending longitudinal processes and expressing a weak NG2-DsRed fluorescence. Despite the relatively abrupt disappearance of NG2-DsRed expression at the junction between PCVs and venules, pericytes in the two segments developed 'propagated' spontaneous Ca^{2+} transients at a similar frequency. Arterioles were wrapped by tightly-packed, circumferentially-arranged smooth muscle cells expressing NG2-DsRed florescence as reported previously (Mitsui & Hashitani, 2013). Densely packed pericytes in PCAs that had a bump-on-a-log appearance with comb-like processes also expressed NG2-DsRed florescence, whereas more sparsely distributed NG2(+) capillary pericytes extended long bipolar processes. Such morphological characteristics in the different microvascular units are very similar to those in the ureteric microvascular network (Borysova *et al.* 2013), mammary gland (Fujiwara & Uehara, 1984) or CNS (Matsushita & Puro, 2006; Hill *et al.* 2015). In capillaries and PCAs, NG2(+) pericytes developed nearly-synchronous spontaneous Ca^{2+} transients at a similar frequency that was lower than that of pericytes in PCVs or venules, although Ca^{2+} transients in PCA pericytes seldom spread into NG2(+) SMCs in the arterioles.

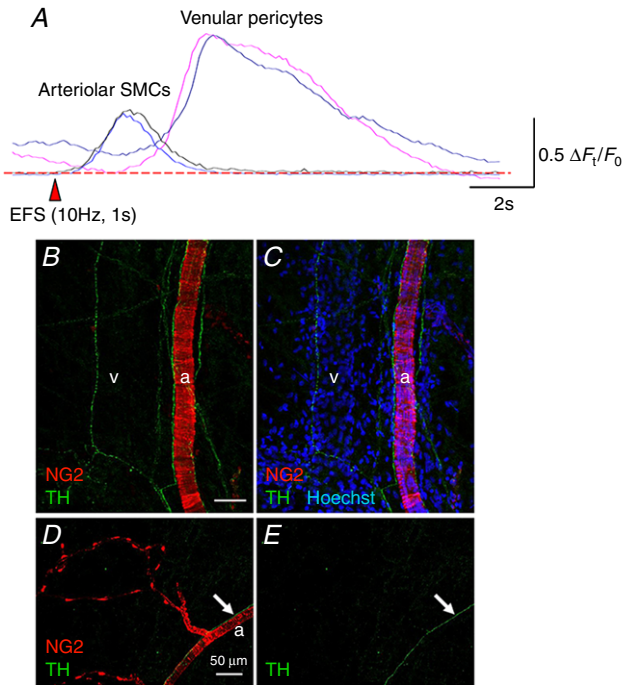

Figure 10. Sympathetic innervation to the suburothelial microvascular network
Electrical filed stimulation (10 Hz, 1s) evoked rapid Ca^{2+} transients in arteriolar smooth muscle cells, whereas slowly developed Ca^{2+} transients were induced in venular pericytes (*A*). In a suburothelial preparation of NG2 DsRed mouse bladder, sympathetic nerve fibres revealed by TH immunoreactivity (green) projected to both an arteriole (a) covered with NG2(+) smooth muscle cells and a venule that did not express an NG2 signal (v) (*B* and *C*). Nucleus staining with Hoechst (blue) indicated the location of the venule. Sympathetic nerve fibres run along an arteriole (a, arrows) covered with NG2(+) smooth muscle cells but did not project to the capillary wrapped by NG2(+) pericytes (*D* and *E*). The scale bars indicate 50 μm (*B* and *D*). [Colour figure can be viewed at wileyonlinelibrary.com]

Role of LVDCCs and TVDCCs

Intercellular spread of LVDCC-dependent regenerative action potentials appears to be a ubiquitous mechanism for maintaining the synchrony of cytosolic Ca^{2+} oscillators in individual vascular SMCs, resulting in vasomotion (Aalkjær & Nilsen, 2005). The synchrony of spontaneous Ca^{2+} transients amongst venular pericytes or SMCs is disrupted by the blockade of LVDCCs (Hashitani *et al.* 2010; Hashitani *et al.* 2012; Mitsui & Hashitani, 2015). In the present study, the synchrony of spontaneous Ca^{2+} transients in NG2(+) pericytes of PCVs and PCAs was indeed disrupted by LVDCC blockade, although LVDCC blockade shortened spontaneous Ca^{2+} transients in NG2(+) capillary pericytes without disrupting their synchrony. The role of LVDCCs in maintaining the synchrony of spontaneous Ca^{2+} transients in NG2(+) pericytes of PCAs and PCVs was further confirmed by the restoration of synchrony with an LVDCC activator. Thus, it appears that Ca^{2+} entry through LVDCCs is essential for the synchrony amongst NG2(+) pericytes in PCAs, PCVs and NG2(−) pericytes in venules (Fig. 11), whereas LVDCC independent depolarizations may be sufficiently large to electrically couple NG2(+) capillary pericytes with each other (Fig. 11).

In venules, spontaneous slow waves were generated at a frequency similar to spontaneous Ca^{2+} transients in NG2(−) venular pericytes. LVDCC blockade prevented slow wave generation leaving STDs that appear to be generated by asynchronous Ca^{2+} transients and subsequent opening of CaCCs (see below). Thus, the opening of LVDCCs triggered by STDs causes slow waves that are readily spread within the NG2(−) venular pericyte syncytium because of their regenerative nature (Fig. 11).

TVDCCs and not LVDCCs appear to be involved in the synchrony of spontaneous Ca^{2+} transients in capillary pericytes in the myenteric plexus of the guinea-pig stomach (Hashitani *et al.* 2015). However, in the bladder suburothelium pretreated with nifedipine, the synchrony of LVDCC-resistant spontaneous Ca^{2+} transients amongst NG2(+) capillary pericytes was not disrupted by Ni 100 μM. In submucosal arterioles of the rat rectum, LVDCC-resistant spontaneous Ca^{2+} transients in mural cells are slowed upon TVDCC blockade without disrupting their synchrony (Mitsui & Hashitani, 2017). Thus, the contribution of either LVDCCs or TVDCCs to the synchrony of spontaneous Ca^{2+} transients amongst mural cells appears to be varied in a vascular bed specific manner.

The termination of spontaneous Ca^{2+} transients at the PCA-arteriolar junction is probably a result of the hyperpolarized membrane potential of arteriolar SMCs (around –70 mV) and thus there may be an abrupt drop in the membrane potentials at the junction between the PCA and the arterioles (Fig. 11). Blockade of inward rectifier K^+ channels with Ba^{2+} depolarized the membrane by ~30 mV, suggesting that inward rectifier K^+ channels play a fundamental role in stabilizing SMC excitability and may preferentially be expressed in arterioles as in the case of other microvascular beds (Matsushita & Puro, 2006; Longden *et al.* 2016). Moreover, voltage dissipation at the branch point between a capillary and its tertiary arteriole was reported in the retinal microvasculature (Zhang *et al.* 2011).

Role of CaCCs and gap junctions

In capillaries, the synchrony of LVDCC/TVDCC-resistant Ca^{2+} transients in NG2(+) pericytes was disrupted by DIDS, a known blocker of CaCCs, suggesting that CaCCs play a critical role in maintaining their synchrony (Fig. 11). A similar role of CaCCs has been reported in the submucosal arterioles of the rat rectum, where the synchrony of mural cells was disrupted by lowering extracellular chloride ion concentration or CaCC blockade (Mitsui & Hashitani, 2017). The fundamental role of CaCCs but not VDCCs in generating spontaneous activity was also proposed in the irideal arterioles (Haddock *et al.* 2002), where voltage independent coupled oscillators may be operated to generate vasomotion (Haddock & Hill, 2005). Gap junction blockade disrupted or

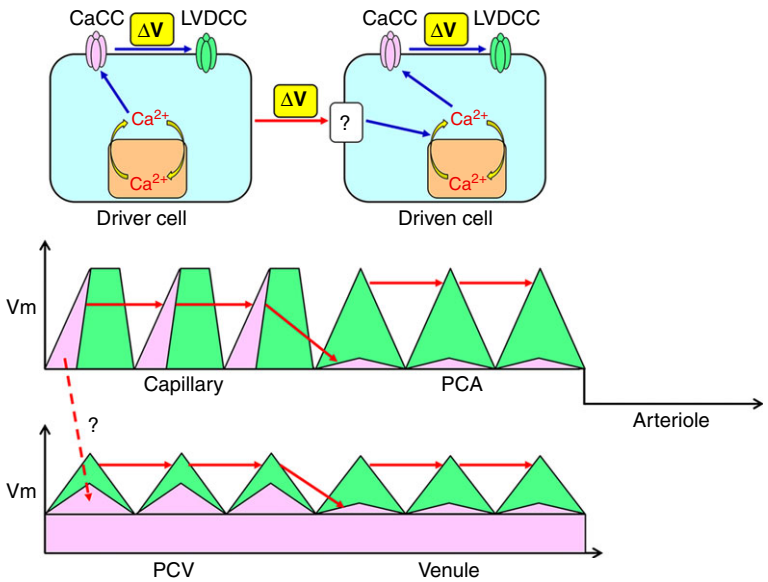

Figure 11. Proposed model of voltage-dependent coupling cytosolic Ca^{2+} oscillators
Driver cells are capable of operating a 'spontaneous' cytosolic Ca^{2+} oscillator that is linked with CaCCs to cause a depolarization triggering the activation of LVDCCs. By contrast, driven cells require depolarizing input from driver cells. The depolarizing input activates cytosolic Ca^{2+} oscillator presumably by voltage-dependent IP_3 production resulting in the activation of CaCCs and VDCCs. Capillary pericytes act as 'driver cells' and generate CaCC-depolarizations that are sufficiently large to couple with each other. PCA pericytes are driven by a spread of the depolarization via gap junctions that activate LVDCCs to couple with each other. The hyperpolarized membrane of arteriolar SMCs prevents the sequential spread of oscillations. Capillary pericytes may also electrically drive PCV pericytes. Upon the background CaCC conductance, a population of PCV pericytes could act as driver cells and generate CaCC-depolarizations, although they require LVDCC activation to couple with each other. Venular pericytes could be driven by a spread of the depolarization via gap junctions that activate LVDCCs to couple with each other. [Colour figure can be viewed at wileyonlinelibrary.com]

diminished the synchrony of spontaneous Ca^{2+} transients amongst NG2(+) capillary pericytes, indicating that the intercellular coupling between capillary pericytes appears to be tight despite the point contact between the longitudinal processes of adjacent pericytes. Alternatively, the electrical coupling between capillary pericytes may be predominantly mediated via the endothelium. The role of the endothelium in maintaining intercellular coupling amongst pericytes has been reported in other vascular beds (Zhang *et al.* 2011, 2013, 2014).

Interestingly, the blockade of either CaCCs or gap junctions invariably prevented the generation of spontaneous Ca^{2+} transients in NG2(+) pericytes in PCAs. Thus, the NG2(+) pericytes in capillary appear to be located upstream of NG2(+) pericytes in PCAs in term of the generation of spontaneous Ca^{2+} transients (Fig. 11). Because CaCC or gap junction blockade blocked spontaneous Ca^{2+} transients in NG2(–) pericytes in venules but not NG2(+) pericytes in PCVs, PCV pericytes appear to be located upstream of venular pericytes. However, whether PCV pericytes may be driven by capillary pericytes or have their own automaticity was not determined. In the venules, blockade of CaCCs with niflumic acid, another known blocker of CaCCs, largely suppressed STDs associated with a membrane hyperpolarization, suggesting that CaCCs contribute not only to the generation of STDs, but also to the relatively depolarized membrane potentials. Because levcromakalim, a K_{ATP} channel opener, hyperpolarized the venular membrane and also prevented the generation of slow waves without leaving STDs, a relatively depolarized membrane as a result of the opening of CaCCs appears to be fundamental for generating spontaneous Ca^{2+} transients presumably by constitutive, voltage-dependent IP_3 production (van Helden & Imtiaz, 2003; Imtiaz *et al.* 2007) (Fig. 11).

Role of SR/ER Ca^{2+} handling

Despite the heterogeneity in the ionic mechanisms maintaining intercellular coupling in different segments of the suburothelial microvasculature, spontaneous Ca^{2+} transients in all segments were abolished by the blockade of SR/ER Ca^{2+} ATPase, indicating that Ca^{2+} handling by SR/ER plays a primary role in the initiation of the spontaneous Ca^{2+} transients. Uptake and release from SR/ER Ca^{2+} stores are well established as mechanisms underlying spontaneous activity in all segments of microvascular units (Aalkjær & Nilsson, 2005; Haddock & Hill, 2005; Hashitani & Lang, 2015). In microvascular units of the bladder suburothelium, NG2(+) capillary pericytes appear to function as 'driver cells', although a population of NG2(+) PCV pericytes are also capable of generating spontaneous Ca^{2+} transients. Thus, NG2(+) pericytes in capillaries and PCVs appear to operate a spontaneous cytosolic Ca^{2+} oscillator linked with membrane CaCCs (Fig. 11). NG2(+) pericytes in PCAs and NG2(–) venular pericytes also have their own cytosolic Ca^{2+} oscillator but require the input of depolarization from 'driver cells' (Fig. 11). This notion is supported by the fact that SMCs or pericytes in a variety of vascular beds are not spontaneously active but are capable of generating oscillatory activity upon agonist stimulation or LVDCC activation (Aalkjær & Nilsson, 2005; Haddock & Hill, 2005; Borysova *et al.* 2013).

In the suburothelial venules, spontaneous Ca^{2+} transients in venular pericytes are abolished by blockers of IP_3-induced Ca^{2+} release but not ryanodine, suggesting that IP_3 receptors rather than ryanodine receptors (RYRs) play a predominant role in the spontaneous SR/ER Ca^{2+} transients (Hashitani *et al.* 2012). In NG2(+) pericytes of PCAs, capillaries or PCVs in the same microvascular unit, spontaneous Ca^{2+} transients were prevented or inhibited by both caffeine and tetracaine, a known blocker of CICR (Thomas & Williams, 2012), suggesting that CICR via RYRs is also involved in the spontaneous SR/ER Ca^{2+} transients in NG2(+) pericytes distributed in these microvascular segments. Therefore, there may be heterogeneity in the role of RYRs in different microvascular segments. In isolated colonic myocytes, IP_3-mediated Ca^{2+} release does not activate RYRs but RYR blockers can inhibit IP_3-mediated Ca^{2+} signals (MacMillan *et al.* 2005). Thus, there appears to be a limitation in discriminating IP_3-induced and RYR-mediated Ca^{2+} release using pharmacological blockers, such as tetracaine, caffeine or 2-aminoethoxydiphenyl borate (Mitsui & Hashitani, 2015), which exerts multiple effects, particularly in multicellular tissue preparations.

Contractility and α-SMA expression

In the suburothelial microvascular unit, α-SMA was strongly expressed in the NG2(+) arteriolar SMCs and NG2(–) venular pericytes, as well as NG2(+) pericytes in PCAs, where increases in $[Ca^{2+}]_i$ were associated with vasoconstrictions. By contrast, NG2(+) pericytes in capillaries did not express α-SMA and were not contractile, whereas the expression of α-SMA and contractility in the NG2(+) PCV pericytes gradually decreased as the diameter was reduced. Similar heterogeneity in the α-SMA and contractility was reported in the microvascular units of the CNS (Nehls & Drenckhahn, 1991; Hall *et al.* 2015). However, several studies reported that capillary pericyte in the CNS (e.g., brain and retina) (Peppiatt *et al.* 2006; Femández-Klett *et al.* 2010; Hall *et al.* 2014) or heart (O'Farrell et al. 2017) are contractile. Thus, capillary pericytes in the bladder suburothelium may function as a driver of other contractile segments to

regulate capillary blood flow rather than having their own contractile machinery to alter capillary diameter.

Sympathetic innervation

NG2(+) arteriolar SMCs that did not develop spontaneous Ca^{2+} transients generated a rapid Ca^{2+} transient associated with a vigorous constriction upon excitations of perivascular sympathetic nerves, as is the case in the rat suburothelial microvasculature (Shimizu et al. 2014). Consistently, TH immunoreactive sympathetic nerves run along the arterioles, as well as the venules, in which NG2(–) pericytes also responded to nerve stimulation by generating a slowly developed contraction. Unlike these larger microvascular segments, NG2(+) pericytes with a bump-on-a-log appearance in the PCAs–capillaries–PCVs complex did not respond to nerve stimulation. This lack of nerve-evoked Ca^{2+} transients or contractions was consistent with their lack of TH-immunoreactive perivascular sympathetic nerves. An *in vivo* study in mesenteric vasculature demonstrated that arteries, terminal arterioles or veins but not PCAs, capillaries or venules less than 30 μm in internal diameter do not respond to perivascular nerve stimulation (Furness & Marshall, 1974). This is in marked contrast to capillary pericytes in the CNS that are under tight neuronal regulation such that the pericytes are capable of regulating regional blood flow to meet the metabolic demands of active neurons (Hall *et al.* 2014; Biesecker *et al.* 2016). Thus, NG2(+) capillary pericytes in the bladder suburothelium may intrinsically control the basal microvascular resistance using their spontaneous Ca^{2+} transients.

Physiological aspects

Spontaneous Ca^{2+} transients in mural cells (i.e. pericytes and smooth muscle cells) and associated vasoconstrictions have been reported in the microvasculature of visceral organs that undergo considerable wall distention upon filling or compression by luminal contents, such as the urinary bladder (Hashitani et al. 2011; Hashitani et al. 2012), stomach (Mitsui & Hashitani, 2015, 2016; Hashitani et al. 2015), colon (Mitsui et al. 2013) or rectum (Mitsui & Hashitani, 2017). Thus, it was envisaged that stretching of the microvasculature may induce or facilitate spontaneous activity of mural cells by opening stretch-activated cation channels to stimulate cytosolic Ca^{2+} oscillator. Because stretching the sheet-like preparations is fundamentally required for fluorescence Ca^{2+} imaging, observed spontaneous activity *in vitro* may not be very similar to that occurring *in vivo*, particularly when the visceral organs are not filled by luminal contents. Metabolic factors (e.g. oxygen concentration or pH) would also affect spontaneous Ca^{2+} activity in mural cells. In arterioles of hamster cheek pouches *in vivo*, increasing oxygen concentrations in perfusate depolarizes the membrane and induces oscillatory vasomotion or sustained constrictions (Welsh *et al.* 1998; Bartlett *et al.* 2000). In the microvasculature of the bladder suburothelium, lowering oxygen concentration in perfusate by bubbling with 95% N_2 and 5% CO_2 did not alter the parameters of spontaneous Ca^{2+} transients in pericytes of all microvascular segments, although the previously measured oxygen concentration under this condition is still higher than the tissue oxygen concentration (Nakamura et al. 2009).

The lower frequency of spontaneous Ca^{2+} transients in capillary pericytes compared with PCV pericytes (Fig. 3*K*) raises the question of the role of capillary pericytes as a dominant driver of spontaneous activity in the suburothelial microvascular unit. Theoretically, the cells generating the highest frequency of spontaneous electrical activity act as a dominant pacemaker within a syncytium as in the case of well-established cardiac pacemaker (Schram *et al.* 2002) or gastric pacemaker (Hashitani *et al.* 2005). Because Ca^{2+} imaging was carried out in urothelium-removed preparations, the microvascular network studied was detached from the extensive capillary network located just beneath the urothelium (Fig. 1*A*–*C*). Such an extensive capillary network may indicate the highest energetic demands in the region and thus pericytes in the capillary network may function as a dominant driver of the suburothelial microvascular unit. In addition, the capillary–PCV connection was not well preserved compared to the capillary–PCA connection, presumably as a result of their fragility. Thus, we were not able to determine whether the capillary pericytes may also drive spontaneous Ca^{2+} signalling in PCVs-venules, or whether there may be transition in terms of the frequency of spontaneous activity in pericytes along the capillaries.

It might be assumed that the long-lasting Ca^{2+} transients (~20s) in capillary pericytes triggering Ca^{2+} transients and associate constrictions in PCA pericytes (Fig. 3*J*) may reduce rather than facilitate capillary perfusion. In the suburothelial preparations gassed with 95% N_2 + 5% CO_2, spontaneous Ca^{2+} transients in pericytes of capillaries/PCAs occasionally spread into SMC-covered arterioles to trigger vigorous constrictions (Hashitani H, unpublished observations). On such occasions, the duration of arteriolar constrictions and associated Ca^{2+} transients (less than 10 s) is much shorter than that of Ca^{2+} transients in neighbouring capillary/PCA pericytes, presumably as a result of the expression of voltage- and/or Ca^{2+}-activated K^+ channels in arteriolar SMCs closing the LVDCC earlier. Precise investigations of PCA/arteriolar constrictions, particularly their time course, at a physiological tissue oxygen concentration are

required. Of particular interest is whether the long-lasting Ca^{2+} transients may be shortened under conditions where spontaneous Ca^{2+} transients are generated at higher frequencies in capillary/PCA pericytes that have communications with the capillary network located just beneath the urothelium.

Clinical implications

There is growing evidence indicating that capillaries or capillary pericytes play a critical role not only in regulating physiological microcirculation, but also in the pathology of diseases in the CNS (Yemisci *et al.* 2009; Hall *et al.* 2014; Ivanova *et al.* 2017) and heart (O'Farrell *et al.* 2017). No-flow phenomenon after catheterization treatments for various cerebral or cardiac ischaemic diseases appears to be attributable to rigor mortis in dead capillary pericytes. In the retina, hypoxia-induced opening of K_{ATP} channels that are predominantly expressed in capillary pericytes (Ishizaki *et al.* 2009) initially dilates the upstream arterioles to increase regional blood flow by suppressing the activity of LVDCCs that are predominantly expressed in arterioles (Matsushita *et al*, 2010). However, this opening of K_{ATP} channels increases Ca^{2+} influx as the driving force of LDVCCs increases into the pericytes and eventually causes their death.

In the bladder microvasculature, the rigor mortis in dead capillary pericytes may also result in capillary constrictions, although normal pericytes in the capillary appear to be intrinsically non-contractile. Diminished spontaneous phasic constrictions in contractile segments of the microvascular units would also deteriorate capillary–tissue exchange. Spontaneous phasic constrictions in arterioles are considered to reduce the blood flow resistance (Meyer *et al.* 2002), whereas diminished vasomotion in retinal arterioles was reported in patients with diabetic retinopathy (Bek *et al.* 2013). Spontaneous constrictions in venules may facilitate venular drainage (Dongaonkar *et al.* 2012). In skeletal muscle, increased tone in PCVs and venules in rat models with metabolic syndrome was reported and it was suggested to contribute to the altered capillary exchange (Lemaster *et al.* 2017).

Overactive bladder (OAB) has been recognized as a consequence of bladder ischaemia, although the precise pathological mechanisms underlying 'ischaemic' OAB remain to be determined (Andersson *et al.* 2014; Thurmond *et al.* 2016; Andersson *et al.* 2017). The beneficial effects of α-adrenoceptor antagonists, β3-adrenoceptor agonists or PDE5 inhibitors on bladder storage symptoms may be attributed to an improvement of the bladder microcirculation. Indeed, these pharmacological agents improve bladder storage function without improving the narrowed luminal diameter of the feeding arteries (Andersson et al. 2014). Thus, it is envisaged that capillary pericytes regulating the integrated contractility of the microvascular unit may play a critical role in developing OAB and provide a potential therapeutic target.

References

Aalkjaer C & Nilsson H (2005). Vasomotion: cellular background for the oscillator and for the synchronization of smooth muscle cells. *Br J Pharmacol* **144**, 605–616.

Andersson KE, Boedtkjer DB & Forman A (2017). The link between vascular dysfunction, bladder ischemia, and aging bladder dysfunction. *Ther Adv Urol* **9**, 11–27.

Andersson KE, Nomiya M, Sawada N & Yamaguchi O (2014). Pharmacological treatment of chronic pelvic ischemia. *Ther Adv Urol* **6**, 105–114.

Bartlett IS1, Crane GJ, Neild TO & Segal SS (2000). Electrophysiological basis of arteriolar vasomotion in vivo. *J Vasc Res* **37**, 568–575.

Biesecker KR, Srienc AI, Shimoda AM, Agarwal A, Bergles DE, Kofuji P & Newman EA (2016). Glial cell calcium signaling mediates capillary regulation of blood flow in the retina. *J Neurosci* **36**, 9435–9445.

Bek T, Jeppesen P & Kanters JK (2013). Spontaneous high frequency diameter oscillations of larger retinal arterioles are reduced in type 2 diabetes mellitus. *Invest Ophthalmol Vis Sci* **54**, 636–640.

Birder L & Andersson KE (2013). Urothelial signaling. *Physiol Rev* **93**, 653–680.

Borysova L, Wray S, Eisner DA & Burdyga T (2013). How calcium signals in myocytes and pericytes are integrated across in situ microvascular networks and control microvascular tone, *Cell Calcium* **54**, 163–174.

Burdyga T & Borysova L (2014). Calcium signalling in pericytes. *J Vasc Res* **51**, 190–199.

Dongaonkar RM, Quick CM, Vo JC, Meisner JK, Laine GA, Davis MJ & Stewart RH (2012). Blood flow augmentation by intrinsic venular contraction in vivo. *Am J Physiol Regul Integr Comp Physiol* **302**, R1436–R1442.

Ellis CG, Wrigley SM & Groom AC (1994). Heterogeneity of red blood cell perfusion in capillary networks supplied by a single arteriole in resting skeletal muscle. *Circ Res* **75**, 357–368.

Fernández-Klett F, Offenhauser N, Dirnagl U, Priller J & Lindauer U (2010). Pericytes in capillaries are contractile in vivo, but arterioles mediate functional hyperemia in the mouse brain. *Proc Natl Acad Sci U.S.A* **107**, 22290–22295.

Fujiwara T & Uehara Y (1984). The cytoarchitecture of the wall and the innervation pattern of the microvessels in the rat mammary gland, a scanning electron microscopic observation. *Am J Anat* **170**, 39–54

Furness JB & Marshall JM (1974). Correlation of the directly observed responses of mesenteric vessels of the rat to nerve stimulation and noradrenaline with the distribution of adrenergic nerves. *J Physiol* **239**, 75–88.

Grundy D (2015). Principles and standards for reporting animal experiments in The Journal of Physiology and Experimental Physiology. *J Physiol* **593**, 2547–2549.

Haddock RE & Hill CE (2005). Rhythmicity in arterial smooth muscle. *J Physiol* **566**, 645–656.

Haddock RE, Hirst GD & Hill CE (2002). Voltage independence of vasomotion in isolated irideal arterioles of the rat. *J Physiol* **540**, 219–229.

Hall CN, Reynell C, Gesslein B, Hamilton NB, Mishra A, Sutherland BA, O'Farrell FM, Buchan AM, Lauritzen M & Attwell D (2014). Capillary pericytes regulate cerebral blood flow in health and disease. *Nature* **508**, 55–60.

Hashitani H & Lang RJ (2016). Spontaneous activity in the microvasculature of visceral organs: role of pericytes and voltage-dependent Ca^{2+} channels. *J Physiol* **594**, 555–565.

Hashitani H, Mitsui R, Masaki S & Van Helden DF (2015). Pacemaker role of pericytes in generating synchronized spontaneous Ca^{2+} transients in the myenteric microvasculature of the guinea-pig gastric antrum. *Cell Calcium* **58**, 442–456.

Hashitani H, Mitsui R, Shimizu Y, Higashi R & Nakamura K (2012). Functional and morphological properties of pericytes in suburothelial venules of the mouse bladder. *Br J Pharmacol* **167**, 1723–1736.

Hashitani H, Takano H, Fujita K, Mitsui R & Suzuki H (2011). Functional properties of suburothelial microvessels in the rat bladder. *J Urol* **185**, 2382–2391.

Hashitani H, Garcia-Londoño AP, Hirst GD & Edwards FR (2005). Atypical slow waves generated in gastric corpus provide dominant pacemaker activity in guinea pig stomach. *J Physiol* **569**, 459–465.

Hill RA, Tong L, Yuan P, Murikinati S, Gupta S & Grutzendler J (2015). Regional blood flow in the normal and ischemic brain is controlled by arteriolar smooth muscle cell contractility and not by capillary pericytes. *Neuron* **87**, 95–110.

Hirose K, Iino M & Endo M (1993). Caffeine inhibits Ca^{2+}-mediated potentiation of inositol 1,4,5-trisphosphate-induced Ca^{2+} release in permeabilized vascular smooth muscle cells. *Biochem Biophys Res Commun* **194**, 726–732.

Imtiaz MS, Zhao J, Hosaka K, von der Weid P-Y, Crowe M & Van Helden DF (2007). Pacemaking through Ca^{2+} stores interacting as coupled oscillators via membrane depolarization. *Biophys J* **92**, 3843–3861.

Ishizaki E, Fukumoto M & Puro DG (2009). Functional K_{ATP} channels in the rat retinal microvasculature: topographical distribution, redox regulation, spermine modulation and diabetic alteration. *J Physiol* **587**, 2233–2253.

Ivanova E, Kovacs-Oller T & Sagdullaev BT (2017). Vascular pericyte impairment and connexin43 gap junction deficit contribute to vasomotor decline in diabetic retinopathy. *J Neurosci* **37**, 7580–7594.

Kawamura H, Sugiyama T, Wu DM, Kobayashi M, Yamanishi S, Katsumura K & Puro DG (2003). ATP: a vasoactive signal in the pericyte-containing microvasculature of the rat retina. *J Physiol* **551**, 787–799.

Lemaster KA, Farid Z, Brock RW, Shrader CD, Goldman D, Jackson DN & Frisbee JC (2017). Altered post-capillary and collecting venular reactivity in skeletal muscle with metabolic syndrome. *J Physiol* **595**, 5159–5174.

Longden TA, Hill-Eubanks DC & Nelson MT (2016). Ion channel networks in the control of cerebral blood flow. *J Cereb Blood Flow Metab* **36**, 492–512.

MacMillan D, Chalmers S, Muir TC & McCarron JG (2005). IP_3-mediated Ca^{2+} increases do not involve the ryanodine receptor, but ryanodine receptor antagonists reduce IP_3-mediated Ca^{2+} increases in guinea-pig colonic smooth muscle cells. *J Physiol* **569**, 533–544.

Matsushita K, Fukumoto M, Kobayashi T, Kobayashi M, Ishizaki E, Minami M, Katsumura K, Liao SD, Wu DM, Zhang T & Puro DG (2010). Diabetes-induced inhibition of voltage-dependent calcium channels in the retinal microvasculature: role of spermine. *Invest Ophthalmol Vis Sci* **51**, 5979–5990.

Matsushita K & Puro DG (2006). Topographical heterogeneity of K_{IR} currents in pericyte-containing microvessels of the rat retina: effect of diabetes. *J Physiol* **573**, 483–495.

Meyer C, de Vries G, Davidge ST & Mayes DC (2002). Reassessing the mathematical modeling of the contribution of vasomotion to vascular resistance. *J Appl Physiol* **92**, 888–889.

Mishra A, Reynolds JP, Chen Y, Gourine AV, Rusakov DA & Attwell D (2016). Astrocytes meditate neurovascular signaling to capillary pericytes but not to arterioles. *Nat Neurosci* **19**, 1619–1627.

Mitsui R & Hashitani H (2017). Properties of synchronous spontaneous Ca^{2+} transients in the mural cells of rat rectal arterioles. *Pflugers Arch* **469**, 1189–1202.

Mitsui R & Hashitani H (2016). Mechanisms underlying spontaneous constrictions of postcapillary venules in the rat stomach. *Pflugers Arch* **468**, 279–291.

Mitsui R & Hashitani H (2015). Functional properties of submucosal venules in the rat stomach. *Pflugers Arch* **467**, 1327–1342.

Mitsui R & Hashitani H (2013). Immunohistochemical characteristics of suburothelial microvasculature in the mouse bladder. *Histochem Cell Biol* **140**, 189–200

Mitsui R, Miyamoto S, Takano H & Hashitani H (2013). Properties of submucosal venules in the rat distal colon. *Br J Pharmacol* **170**, 968–977

Nakamura E, Yokoi T, Fukuta H, Iida T, Tanaka Y, Yamamoto Y & Suzuki H (2009). Hypoxia differentially modulates the activity of pacemaker and smooth muscle cells in the guinea pig stomach antrum *J Smooth Muscle Res* **45**, 149–166.

Nehls V & Drenckhahn D (1991). Heterogeneity of microvascular pericytes for smooth muscle type alpha-actin. *J Cell Biol* **113**, 147–154.

O'Farrell FM, Mastitskaya S, Hammond-Haley M, Freitas F, Wah WR & Attwell D (2017). Capillary pericytes mediate coronary no-reflow after myocardial ischaemia. *Elife* **6**, e29280.

Peppiatt CM, Howarth C, Mobbs P & Attwell D (2006). Bidirectional control of CNS capillary diameter by pericytes. *Nature* **443**, 700–704.
Peng H, Matchkov V, Ivarsen A, Aalkjaer C & Nilsson H (2001). Hypothesis for the initiation of vasomotion. *Circ Res* **88**, 810–815.
Sakagami K, Wu DM & Puro DG (1999). Physiology of rat retinal pericytes: modulation of ion channel activity by serum-derived molecules. *J Physiol* **521**, 637–650.
Sakurai T & Terui N (2006). Effects of sympathetically induced vasomotion on tissue-capillary fluid exchange. *Am J Physiol Heart Circ Physiol* **291**, H1761–H1767.
Schram G, Pourrier M, Melnyk P & Nattel S (2002). Differential distribution of cardiac ion channel expression as a basis for regional specialization in electrical function. *Circ Res* **90**, 939–950.
Segal SS & Bény JL (1992). Intracellular recording and dye transfer in arterioles during blood flow control. *Am J Physiol Heart Circ Physiol* **263**, H1–H7.
Shimizu Y, Mochizuki S, Mitsui R & Hashitani H (2014). Neurohumoral regulation of spontaneous constrictions in suburothelial venules of the rat urinary bladder. *Vascul Pharmacol* **60**, 84–94.
Thomas NL & Williams AJ (2012). Pharmacology of ryanodine receptors and Ca^{2+}-induced Ca^{2+} release. *WIREs Membr Transp Signal* **1**, 383–397.
Thurmond P, Yang JH & Azadzoi KM (2016). LUTS in pelvic ischemia: a new concept in voiding dysfunction. *Am J Physiol Renal Physiol* **310**, F738–F743
Van Helden DF & Imtiaz MS (2003). Ca^{2+} phase waves: a basis for cellular pacemaking and long-range synchronicity in the guinea-pig gastric pylorus. *J Physiol* **548**, 271–296.
Villringer A, Them A, Lindauer U, Einhäupl K & Dirnagl U (1994). Capillary perfusion of the rat brain cortex.An in vivo confocal microscopy study. *Circ Res* **75**, 55–62.
Welsh DG, Jackson WF & Segal SS (1998). Oxygen induces electromechanical coupling in arteriolar smooth muscle cells: a role for L-type Ca^{2+} channels. *Am J Physiol Heart Circ Physiol* **274**, H2018–H2024.
Yemisci M, Gursoy-Ozdemir Y, Vural A, Can A, Topalkara K & Dalkara T (2009). Pericyte contraction induced by oxidative-nitrative stress impairs capillary reflow despite successful opening of an occluded cerebral artery. *Nat Med* **15**, 1031–1037.
Zhang T, Wu DM, Xu GZ & Puro DG (2011). The electrotonic architecture of the retinal microvasculature: modulation by angiotensin II. *J Physiol* **589**, 2383–2399.
Zhang Z, Lin H, Cao C, Payne K & Pallone TL (2014). Descending vasa recta endothelial cells and pericytes form mural syncytia. *Am J Physiol Renal Physiol* **306**, F751–F763.
Zhang Z, Payne K & Pallone TL (2013). Syncytial communication in descending vasa recta includes myoendothelial coupling. *Am J Physiol Renal Physiol* **307**, F41–F52.
Zhu X, Bergles DE & Nishiyama A (2008). NG2 cells generate both oligodendrocytes and gray matter astrocytes. *Development* **135**, 145–157.

Additional information

Competing interests

The authors declare that they have no competing interests.

Author contributions

HH was responsible for the conception and design of the experiments. HH, RM, KN and ML were responsible for the collection, analysis and interpretation of data. HH, RM, KN and ML were responsible for drafting the article or revising it critically for important intellectual content. All authors have read and approved the final manuscript submitted for publication and are accountable for all aspects of the work. All persons designated as authors qualify for authorship and all those who qualify are listed.

Funding

The present study was supported by Grant-in-Aid for Challenging Exploratory Research (No. 21659377) from The Japan Society for Promotion of the Science (JSPS) to HH and a research grant from The Nitto Foundation to RM.

Acknowledgements

The authors thank Dr Richard Lang (Monash University) for critically reading the manuscript.

Supporting information

Additional supporting information may be found online in the Supporting Information section at the end of the article.

Video S1. Spontaneous Ca^{2+} transients in PCA pericytes
NG2(+) pericytes in a PCA (shown in Fig. 3*E*) developed synchronous spontaneous Ca^{2+} transients. Frame rate is 100 ms (10 frames s^{-1}).
Video S2. Spontaneous Ca^{2+} transients in capillary pericytes
NG2(+) pericytes in a capillary (shown in Fig. 3*F*) developed nearly-synchronous spontaneous Ca^{2+} transients. Frame rate is 100 ms (10 frames s^{-1}).
Video S3. Spontaneous Ca^{2+} transients in pericytes of capillary network
Pericytes in a capillary network fired spontaneous Ca^{2+} transients that spread one after another from left to right. Frame rate is 100 ms (10 frames s^{-1}).

Video S4. Spontaneous Ca^{2+} transients in PCA-capillary tree
Pericytes in a PCA-capillary tree fired spontaneous Ca^{2+} transients that spread into the PCA to trigger nearly-synchronous Ca^{2+} transients within the PCA-capillary tree. Frame rate is 100 ms (10 frames s^{-1}).
Video S5. Spontaneous Ca^{2+} transients in PCV pericytes
Pericytes in a PCV (shown in Fig.3G) expressing a weak NG2/DsRed fluorescence developed propagated spontaneous Ca^{2+} transients. Endothelial cells also generated asynchronous spontaneous Ca^{2+} transients. Frame rate is 100 ms (10 frames s^{-1}).
Video S6. Spontaneous Ca^{2+} transients in venular pericytes
NG2(–) Pericytes in a venule (shown in Fig.3H) developed propagated spontaneous Ca^{2+} transients. Note that NG2(+) arteriolar SMCs remained quiescent. Frame rate is 100 ms (10 frames s^{-1}).
Video S7. Spontaneous Ca^{2+} transients at a PCV–venular junction
Pericytes in a PCV and a connected venule developed propagated spontaneous Ca^{2+} transients. Frame rate is 100 ms (10 frames s^{-1}).
Video S8. Spontaneous Ca^{2+} transients at a capillary-PCA junction
Pericytes in a capillary developed synchronous spontaneous Ca^{2+} transients that spread into a connected PCA to trigger spontaneous Ca^{2+} transients. Frame rate is 100 ms (10 frames s^{-1}).
Video S9. Effect of gap junction blockade on spontaneous Ca^{2+} transients at a capillary–PCA junction
At the capillary-PCA junction shown in suppl video9 that had been treated with carbenoxolone (10 μM), capillary pericytes still developed nearly-synchronous spontaneous Ca^{2+} transients but failed to trigger PCA Ca^{2+} transients. Frame rate is 100 ms (10 frames s^{-1}).